J Mater Sci (2010) 45:5425–5455
DOI 10.1007/s10853-010-4708-9

REVIEW

Fabrication of ceramic components with hierarchical porosity

Paolo Colombo · Cekdar Vakifahmetoglu · Stefano Costacurta

Received: 27 February 2010 / Accepted: 7 June 2010 / Published online: 26 June 2010

Abstract This article reviews different methodologies for the fabrication of monolithic ceramic components possessing multiscale porosity, i.e., with pores ranging from a few nanometers to several hundred microns. Two main strategies have been discussed: (a) the assembling of micro/mesoporous materials into components possessing also macropores; (b) the addition of micro/mesoporosity to macroporous, cellular monoliths. Both routes include one-pot and multi-step processing routes, and yield components with different properties in terms, for instance, of specific surface area values, mechanical strength, and permeability to fluids. The wide range of processing approaches available enable the fabrication of components with very varied morphology, suitable for a variety of industrial applications.

Abbreviations

BCC	Body-centered cubic
BET	Brunauer, Emmett, Teller (theory for the physical adsorption of gas molecules on a surface used for the determination of SSA)
CAP	Catalyst-assisted pyrolysis
CCVD	Catalytic chemical vapor deposition
CDC	Carbide-derived carbon
cmc	Critical micellar concentration
CNF	Carbon nanofiber
CNT	Carbon nanotube
CTAB	Cetyltrimethylammonium bromide
CVD	Chemical vapor deposition
DNPTES	3-(2,4-dinitrophenylaminopropyl) triethoxysilane
EISA	Evaporation-induced self assembly
F127	Pluronic block copolymer: PEO_{106}-PPO_{70}-PEO_{106}
FCC	Face-centered cubic
LBL	Layer-by-layer
MCF	Mesostructured cellular foam
MTES	Methyltriethoxysilane
P123	Pluronic block copolymer: PEO_{20}-PPO_{70}-PEO_{20}
PCP	Pulsed current processing
PCS	Polycarbosilane
PEG	Poly(ethylene glycol)
PEO	Poly(ethylene oxide)
PMO	Periodic mesoporous organosilica
PPO	Poly(propylene oxide)
PS	Polystyrene
PU	Polyurethane
RVC	Reticulated vitreous carbon
SEM	Scanning electron microscopy
SSA	Specific surface area (typical units: m^2/g)
TEM	Transmission electron microscopy
TEOS	Tetraethoxysilane (tetraethyl orthosilicate)
TLCT	True liquid crystal templating
TMB	Trimethylbenzene
TMOS	Tetramethoxysilane (tetramethyl orthosilicate)
TPAOH	Tetrapropylammonium hydroxide
TTIP	Titanium tetraisopropoxide
UF	Urea-formaldehyde
W/O	Water-in-oil (emulsion)

P. Colombo · C. Vakifahmetoglu
Dipartimento di Ingegneria Meccanica—Settore Materiali, University of Padova, Via Marzolo 9, 35131 Padova, Italy

S. Costacurta
Associazione CIVEN, Via delle Industrie 5, 30175 Venezia, Italy

P. Colombo (✉)
Department of Materials Science and Engineering, The Pennsylvania State University, University Park, PA 16802, USA
e-mail: paolo.colombo@unipd.it

Introduction

In addition to the composition of the ceramic material constituting the solid skeleton of a porous component, the characteristics of its porosity (total amount, ratio closed/open porosity, average pore size and distribution, pore shape, tortuosity and interconnectivity, presence of graded porosity), which are determined by the manufacturing process employed, govern its properties and suitability for potential applications [1]. For instance, micropores are needed for adsorption and purification of a gaseous or liquid stream, while macropores are required in biomedical applications (bone scaffolds). A combination of different pore morphologies in a single monolithic matrix extends the properties of a component, and subsequently widens significantly its range of applications. When porous materials are required to perform multiple functions, hierarchical porosity constitutes a means to accomplish these multiple tasks. For example, micro–macro porosity can greatly improve the performance of microporous materials in applications where a component with both catalytic function and high mechanical strength is required. In general, it can be said that a macroporous ceramic framework offers chemical and mechanical stability, as well as high convective heat transfer, high turbulence, low pressure drop, and a high external mass transfer rate due to interconnections between the macropores [2], while the micro/mesoporous system provide the functionality for a given application.

A porous component containing pores on two or more length scales is referred to as a material with hierarchical porosity. Different types of hierarchical porosity may exist, according to the range of pore sizes that are involved in the porous structure, i.e., bimodal size distribution (micro-meso, meso-macro, micro–macro), or trimodal (micro-meso-macro). Graded or oriented porosity is also sometimes desirable for specialized applications. A component containing hierarchical porosity typically possesses simultaneously a wide range of desirable characteristics, which include high accessibility, rapid transport of fluid and gases, high selectivity, fast uptake and release, the possibility of rapid thermal cycling, chemical and mechanical stability and efficient use of volume. The presence of small pores (particularly micropores) provides a high SSA, i.e., geometric area per unit mass of the part. These components are therefore of significant technological interest, and are successfully used in several industrial processes and household products. Applications include catalysis, filtration (of liquids or gases), extraction, separation, sorption, and scaffolds for biological applications [3, 4]. However, several challenges remain: in particular, limited mechanical strength (especially for components with micro-meso porosity), poor structural control at all length scales, and the requirement of elaborate processing methods to achieve such complex, multiscale microstructures.

In the remainder of the text, we will refer to microporosity when the pore size is <2 nm, mesoporosity when the pore size is between 2 and 50 nm, and macroporosity for pore sizes >50 nm. It must be observed, however, that this terminology used to classify the porosity of materials, which was developed by the International Union of Pure and Applied Chemistry (IUPAC) chiefly with the aim of helping in the characterization of catalytic materials [5], is not particularly of assistance in the description of the porosity of cellular materials. In fact, it defines a porous solid as "a solid with pores, i.e., cavities, channels or interstices, which are deeper than they are wide" (which is not always the case, as for instance in foams) and the pore size (generally pore width) as "the distance between two opposite walls of the pore" (therefore failing to take into account asymmetric pore shapes). More importantly, according to this definition, all cellular ceramics are constituted of macropores, a generalization which does not help in describing the architecture of their porosity in a detailed and meaningful way. The technical literature, however, borrowing from what has been proposed for plastics [6] has started distinguishing between macro-cellular and micro-cellular foams [7], the latter possessing cells with a size smaller than 30–50 μm and a cell density (number of cells per unit volume) greater than 10^9 cells/cm^3. Another publication [8] provides a more accurate description of porosity and methods for its investigation taking into account several parameters, such as pore size and size distribution, pore shape and volume, open or closed porosity.

Several processing routes have been proposed to fabricate ceramic components with hierarchical, multiscale porosity. The synthetic approaches can be roughly divided into two main categories: (1) the assemblage of micro- and mesoporous materials into macroporous monoliths (see Fig. 1) and (2) the production of macroporous ceramics followed by the introduction of micro/mesoporosity (see later, Fig. 4). Both routes include one-pot and multi-step processing strategies, and they are summarized in Fig. 1. Starting from sacrificial templates with different length scales (e.g., polymer or silica spheres, block copolymers, surfactants), which are eventually removed, macroporous architectures with (micro/meso)porous walls are typically generated. Alternatively, if a macroporous material is used as a skeleton for the successive growth/deposition of micro/mesostructures, a hierarchical porous component with "dense" walls is obtained. This distinction was also made by Avila et al. [9], who classified two basic types of monolithic catalyst supports, as "coated" and "incorporated", according to both the component distribution and the preparation method. These two approaches will be discussed in "From micro- and mesoporosity to multiscale

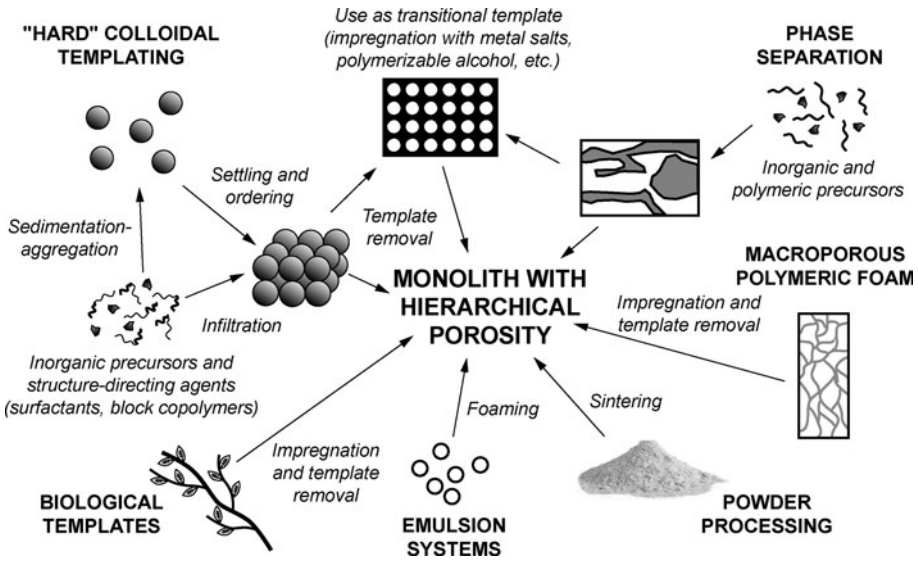

Fig. 1 Fabrication of ceramic components with hierarchical porosity. Processing strategies for adding macroporosity to micro/mesoporous materials

pore hierarchy" and "From macroporosity to multiscale pore hierarchy", respectively.

Since the production of micro- and mesoporous ceramics as well as their combination (i.e., micro–meso hierarchical porosity) has been covered recently by some authors [10–12] this review article will focus mainly on monolithic ceramic components which also contain macroporosity (ranging from a few micrometers to millimeters) in their pore architecture, which can therefore be classified as either bimodal (micro–macro and meso–macro) or trimodal (micro–meso–macro). It should be noted here that in the following text we will not deal with the fabrication of coatings and separate particles, even though they can be produced with multi-scale porosity. Moreover, we will not discuss ceramic membranes, which are asymmetric porous structures composed of a separation film deposited on a ceramic support structure comprising up to five different layers. Depending on the degree of separation required (i.e., micro-, ultra-, hyper-filtration, gas separation, or pervaporation), the pore size ranges from a few angstrom in the top membrane to a few microns in the support (typically < 15 μm). Therefore, such a component possesses hierarchical porosity too [13].

From micro- and mesoporosity to multiscale pore hierarchy

Templating strategies

In his review on high-surface area inorganic materials, Schüth [14] divided the templating approaches used in the synthesis of porous solids into two different categories: endo-templating and exo-templating. In endo-templating, a template is included as an isolated entity into the growing solid; the template is then removed by solvent extraction or calcination, leaving behind a porous solid where pore size and shape reflect the structure of the template. In exo-templating, a porous structure is used as a scaffold in which the voids are filled by a growing structure; if the scaffold is removed after filling of the voids, a porous solid is generated.

Pore size is largely a function of the templating object, e.g., colloidal polymer or silica dispersions give rise to macroporosity [15, 16], whereas surfactants and amphiphilic block copolymers form aggregates (micelles) via self-assembly and yield a mesostructure which can be disordered or have a well-defined periodicity up to tens of nanometers. Single molecules are used as templates for micropore formation in zeolitic materials. The review by Soler-Illia et al. [17] can be considered a milestone on templated micro- and mesoporous oxides.

Strictly speaking, a porogen can be called a "template" only in the case of an univocal relationship between the porogen's own structure and the final structure of the porous material; in other words, a template is always a "hard" object which does not significantly alter its shape when the solid counterpart is being formed [18]. Therefore, important synthetic strategies, such as single-molecule templating for zeolites and self-assembled aggregates for mesoporous materials, are ruled out. The synthesis of mesoporous materials is a highly cooperative process, in which the self-assembly of surfactants occurs during inorganic condensation. The two processes are mutually influenced: mesophase changes and order–disorder transitions, in fact, can be observed during formation of the inorganic phase, for example by in situ techniques [19, 20]. This is especially

evident when kinetics plays a fundamental role, such as in EISA in the fabrication of mesoporous films [21, 22], but even when synthesis is carried out with a stronger thermodynamic control, such as in TLCT [23]. In these cases, the term "structure-directing agent" is to be preferred to "template" [24]. Such structure-directing agents are, e.g., molecular species in zeolite synthesis [25], and microemulsions [26], low-molecular weight surfactants and amphiphilic block copolymers [27, 28] in the synthesis of mesoporous materials. However, in the scope of this review we will adopt a generally accepted terminology, and consider a "template" as a generic porogen structure (either "soft" or "hard"), including polymeric particles, beads, foams and emulsions, templates of biological origin, inorganic salts, etc.

In the production of hierarchical porous cellular ceramics, large templating objects such as colloids, microspheres and emulsions are exploited to create macroporosity at different length scales, from sub-micron to several hundred micrometers and millimeters, whereas mesopores are obtained via supramolecular structures formed from self-assembly of surfactants, and micropores can be generated by the templating effect of single molecules. Alternatively, a preformed macroporous template can be used as a sacrificial scaffold for the growth of a micro-, meso-, or micro-mesophase, yielding a hierarchical porous architecture upon template removal by either calcination or solvent extraction.

Recently, Yuan and Su [29] reviewed most of the synthesis strategies to produce hierarchical meso–macroporous materials. Trimodal micro–meso–macroporous components, for use in catalysis, can be synthesized utilizing combined templating approaches on multiple length scales [30]. In this review, we will focus especially on the production of porous monolithic ceramic with hierarchical macro–meso and macro–micro porosity by different templating approaches (i.e., micro–mesoporosity will not be covered here). In addition, more emphasis will be given to macropore sizes of at least several hundred nanometers, whereas macropore sizes slightly larger than 50 nm have been purposefully disregarded. This is because larger macropores afford better flow properties (e.g., high accessibility, low pressure drop, rapid transport of fluid and gases) to the component, which are of vital importance in applications requiring mass transport, such as catalysis, in comparison to pores with a size limited to a few tens of nanometers.

"Hard" templating

Colloids can be defined as particles with a size sufficiently small (less than 1 μm) not to be affected by gravitational forces, but sufficiently large (more than 1 nm) to show marked deviations from the properties of true solutions [31]. Hierarchical porosity ceramics are obtained by the double templating effect of larger colloidal objects and smaller or supramolecular aggregates, such as surfactants, amphiphilic block copolymers, and ionic liquids. Close-packed arrays of colloidal spheres can be infiltrated with a precursor solution containing the structure-directing agents, which originate the mesopores. Alternatively, a precursor solution containing both macro- and mesoporogens can be used in a one-pot preparation. Various compositions of hierarchical macroporous ceramics with mesoporous walls including titania [32], silica [33, 34], niobia [32], alumina [35–37], and silica-alumina [38] were prepared following these routes.

Colloidal dispersions made of monodisperse spherical particles of several hundred nanometers spontaneously form ordered close-packed crystal structures (typically face-centered cubic (FCC) or BCC) called opals, upon settling on a substrate by slow-speed dip-coating or centrifugation. Because these structures are constituted of regular assemblies of monodisperse spheres with periodicity of the same order of the wavelength of visible light, they diffract light and have an optical band gap, and therefore interesting applications emerge as photonic crystals, for example in sensing and in optoelectronic devices [39–41]. Colloidal crystals can be exploited in the synthesis of macroporous materials if the interparticle voids are filled with a growing phase, for example by impregnation with precursors in liquid phase, such as alkoxides [33] and salt solutions [42], or in vapor phase such as by the CVD process [43]. The spheres are eventually removed by calcination (e.g., in the case of latex particles), solvent extraction, or chemical etching (e.g., by a hydrofluoric acid (HF) treatment in the case of colloidal silica). Different types of cellular macroporous materials can be fabricated by templating with colloidal crystals, in which the macropore size, shape and interconnectivity in such structures is determined by an appropriate choice of the precursor colloids. The general applicability of this templating approach to the preparation of a variety of inorganic and hybrid macroporous structures was demonstrated by Holland et al. [33, 34] who obtained macroporous compositions including oxides of Si, Ti, Zr, Al, W, Fe, Sb, mixed Zr/Y, aluminophosphates and organically functionalized silicates, by infiltration of the colloidal crystal with alkoxides.

In the simplest approach, inorganic precursors in combination with appropriate structure-directing agents (such as surfactants and block copolymers) are allowed to infiltrate the voids between the spheres constituting the colloidal crystal, followed by condensation and removal of the templating spheres and the structure-directing agents. In this way, macroporous ceramics with mesoporous inorganic walls can be obtained, in which the hard spheres

act as the scaffold for the growth of the macroporous walls and the structure-directing agents constitute the mesoporogens [14, 29].

Bimodal pore structures of macropores (250 nm average diameter) surrounded by microporous zeolithic walls were fabricated combining PS sphere templating with the use of TPAOH as the structure-directing agent for the in situ synthesis of the silicalite walls [44]. Sen et al. adopted an infiltration strategy with the purpose to achieve porosity with three-dimensional (3D) interconnectivity, obtaining a multimodal hierarchical structure using PS latex spheres, Pluronic F127 and P123 in the presence of cosurfactants (butanol or pentanol). The resulting hierarchically porous high SSA (531 m^2/g) silica structure presented ordered macropores (200–800 nm) with interconnecting windows (70–130 nm) and ordered mesoporous walls (80 nm) with significant microporosity (<2 nm) [45]. Hierarchically porous alumina was obtained using either silica gel or PS microspheres as the macroporogen and stearic acid as the mesoporogen, though the mesostructure consisted in a disordered pore arrangement [37].

This approach is useful in the synthesis of hybrid macro–mesoporous materials, where an organic moiety is incorporated in the inorganic framework by either weak (e.g., hydrogen bonding) or covalent bonding (e.g., Si–C bond). For example, crystalline arrays of monodisperse PS spheres were fabricated by slow sedimentation and water evaporation of a colloidal suspension. This colloidal crystal was then used as the macrotemplate for the in situ evaporation-induced deposition of organically functionalized mesostructured silica templated by CTAB, containing tetraethoxysilane (TEOS) and 3-(2,4-dinitrophenylaminopropyl)triethoxysilane (DNPTES). A hierarchical porous structure with bimodal pore size distribution was thus obtained upon solvent extraction [46].

Besides addressing the synthesis of silica and other oxides, this approach can be exploited in the preparation of hierarchically porous carbons. A dual-templating strategy was adopted for the direct synthesis of ordered macro–mesoporous carbons [47]: silica colloidal crystals were used as a hard template for the generation of ordered FCC macropore arrays, then a solution containing block copolymer Pluronic F127 as the structure-directing agent and a phenolic resin as the carbon source was allowed to infiltrate the colloidal crystal. The self-assembly of Pluronic F127 into ordered mesostructures occurred in the voids of the silica colloidal crystal, in the presence of the phenolic resin. After drying and pyrolysis at 800 °C in N_2, the composite was treated with HF to etch the silica phase and a carbon monolith with hierarchical macro–mesoporosity was obtained with mesopore size of 11 nm, tunable macropore sizes of 230–430 nm and interconnected macropore windows of 30–65 nm.

Colloidal particles can also be coated with the precursor of the desired material to process before formation of the ordered crystal, in the so-called sedimentation–aggregation technique [48]. In this process, the silica precursor is deposited on PS beads through a homogeneous wetting process, and then the coated particles are used to form a colloidal crystal in which the pores of the opal are incompletely filled. The removal of the spheres, either by calcination or by solvent extraction, leads to the formation of 3D ordered meso–macroporous materials, where mesoporosity is associated with interstitial voids between walls, cracks, and incomplete closures of the silica walls occurring during inorganic condensation and calcination. One advantage provided by pre-coating the beads is that no preordered arrangement of the latex beads is needed, which makes the process simpler, faster, and more suitable for industrial scaleup.

Oh et al. [49] proposed a mechanism for the formation of these skeletal macrostructures involving the formation of "donut-like" building blocks in the interstices of adjacent spheres upon drying of the inorganic precursor. These building blocks arrange into close-packed FCC structures, and the inner space of the "donut-like" building unit creates the interconnecting channels between the macropores. Indeed, a structure-directing agent such as a surfactant can be added to the solution used for coating of the microspheres. Interestingly, if the microspheres are soaked into the surfactant solution before introducing the silica precursor, the microspheres are covered with the amphiphilic surfactant, therefore become hydrophilic and are more easily and homogeneously incorporated into the silica gel, obtaining a uniform dispersion of macropores in the material. This synthetic approach combines the sedimentation–aggregation technique with the liquid crystal templating method [50]. Another variant of this method is based on the LBL deposition of micro- or mesoporous particles on polymeric beads [51]. Silicalite-1 nanoparticles were assembled into core–shell structures by LBL deposition on monodisperse 640-nm diameter PS beads, obtaining deposition of multilayered shells by alternating the deposition of negatively charged silicalite with a polycationic layer of poly(diallyldimethylammonium chloride). The coated PS beads were first centrifuged to obtain ordered arrays and then calcined to remove the organic components, producing a monolithic macroporous silicalite with a pore size of $\sim$500 nm [52].

Meso–macroporous alumina was prepared by coating monodisperse latex spheres of controlled size (300–400 nm) with mesoporous alumina via EISA starting from Pluronic P123 triblock copolymer as the structure-directing agent and aluminum isopropoxide. Contrary to other works, in which alumina with disordered mesoporosity was obtained [37], this procedure was demonstrated to be

suitable for obtaining a well-resolved, hybrid macro–mesophase with hexagonal mesopore structure, which was deposited by sedimentation into a hexagonal or cubic close-packed array, followed by elimination of the supernatant solution and calcination [36].

The approach of infiltrating a colloidal crystal with mesostructured precursors presents the advantage of obtaining close-packed structures with a very high degree of order, if monodisperse spheres are used. Alternatively, if templates with different sizes are used, variable pore hierarchy and graded pore systems can be successfully formed. On the other hand, the close-packed structure obtained in colloidal crystal fabrication does not allow variation of the pore wall and pore interconnections, which are essentially determined by the geometry of the points of contact between the spheres. Furthermore, this is a two-step process which can be time-consuming in both the colloidal crystal formation and the infiltration processes.

One-pot synthetic strategies have been devised, which make use of a dual templating solution, where both the large diameter colloids and the block copolymers are simultaneously present. The macro- and the mesopore templating occur at the same time, in a one-step procedure. In this case, the interface between the inorganic phase and the template must be carefully controlled: whereas in mesostructured materials the coupling between the block copolymers and the silica framework is achieved via hydrogen bonding between the silanols and the ether crown of the PEO chains, for polymeric spheres this bonding must be mediated by appropriate functional groups at the particle surface, therefore surface-functionalized polymer spheres should be used. For example, bimodal pore hierarchy was achieved using a dual templating synthesis using PS spheres and a PS–PEO block copolymer [53]. This work suggests another advantage of this one-step technique: the wall thickness can be controlled independently of the pore size by choosing the relative amount of polymer latex to silica. In this way, because mechanical properties are greatly affected by pore size and wall thickness, the mechanical stability of a hierarchical material can be improved. Another requisite of this strategy is that to obtain a homogeneous distribution of pores in the silica matrix sufficient colloidal stability during the whole condensation reaction and strong particle–particle repulsion are required. In the cited work [53], this was done by steric stabilization of the latex particles by dangling PEO or poly(styrene sulfonate) chains.

The interaction between the block copolymer hydrophilic ends and the inorganic walls can cause the presence of additional micropores in the structure: the hydrophilic ends of the block copolymer extend in the inorganic framework and act as "single molecule" templates, i.e., after template removal, microporosity is generated by the templating effect of single copolymer chain ends. In this way, trimodal micro–meso–macroporosity can be generated [35]. For example, Suzuki et al. [54] recently produced high SSA trimodal porous silica (356 m^2/g) and alumina (329 m^2/g). The obtained products had three pore size distributions: ~200 nm macropores originating from PS spheres, ~4 nm mesopores (cage-type) originating from the triblock copolymer, and <2 nm micropores due to the "single molecule templating effect" of the block copolymer. 3D cubic ordered macroporous (140 nm) and binary macroporous (140, 80 nm) silica structures having ordered mesoporous (7.7 nm) walls have been synthesized using cubic closed-packing colloidal crystals as the templates. The colloidal crystals can be made from equal-sized or binary-sized latex spheres by the simple methods of self-sedimentation on a film or pressing into a pellet [55].

Open-framework zeolite monoliths were prepared using dextran (a polysaccharide with MW = 70000 g/mol) dissolved in water in presence of NaY zeolite crystallites (size range 0.7–1 mm) and silica nanoparticles (14 nm diameter) [56]. Thermal decomposition of the dextran matrix at 270 °C with associated outgassing of steam and carbon dioxide led to the fabrication of expanded carbon-based foam that served as a template for patterning the thermally induced aggregation of silica/zeolite particles. Further heating to 470 and 600 °C resulted in destruction and removal of the carbon foam, forming an inorganic sponge-like monolithic replica (1–2 cm in size). The structure consisted of a continuous open framework of interconnected filaments, about 15 μm in width and 100–150 μm in length, and had limited strength. In other synthesis conditions, closed-framework structures were obtained in which the zeolite particles stabilized the formation of thin self-supporting NaY/silica films across the 100–300-μm sized apertures of the cellular framework [57].

Hard templating is not limited to close packing of hard spheres: indeed, other strategies have been devised to obtain hierarchically porous materials on two or three length scales. In particular, adding mixtures of ionic and non-ionic surfactants of different block lengths should lead to porosity on three length scales. However, this is not necessarily always the case, because the small surfactant often acts as a co-template for the larger one, therefore this strategy normally results in a monomodal pore size rather than the desired bimodal distribution [58]. Mesopore templates other than surfactants have been used, e.g., ionic liquids: these are organic salts with melting points of below ~100 °C, sometimes as low as −96 °C, so they can be used as solvents under conventional organic liquid-phase reaction conditions [59]. Because they have a particular templating behavior attributed to the strong polarizability of the ionic head

group, which leads to a stronger tendency for the formation of self-assembled aggregates, they have been proposed as templates for the synthesis of mesostructured silica, especially in combination with large-molecular weight block copolymers for the synthesis of bimodal mesoporous materials [60, 61]. Bimodal micro (1.3 nm)/macro (175 nm) porous silica was obtained using PS bead packing and an amphiphilic ionic liquid as dual templates; the overall BET surface of the hierarchical porous silica formed in this study was very high (>1000 m^2/g) [62]. Kuang et al. [58] used PS (560 nm particles), a block copolymer and an ionic liquid as the templates to produce a trimodal (meso–meso–macro) porous ceramic. The material possessed a 3D macroporous structure (~360 nm cell size), with long-range order and interconnecting windows of ~80 nm. The surface of the cell walls was shown to contain two types of mesopores: large spherical mesopores (~12 nm) and small elongated mesopores (2–3 nm), leading to high SSA (244 m^2/g).

The utilization of macroporous hard templates obtained by PEG-induced controlled phase separation (see section "Phase separation techniques") to form hierarchical porous ceramics has also been explored, using a nano-casting approach. In this procedure, a porous solid material (typically silica) is used as a hard monolithic exo-template, and its pores are filled with one or more precursor species which react in situ to form the desired material. The exo-template is finally removed (e.g., dissolution in HF in the case of silica, combustion in the case of organic compounds) to yield the product as its negative replica. Structure replication allows synthesizing many ordered porous materials which cannot be synthesized by single templating: for example, only a limited range of mesoporous metal oxides has been successfully prepared using amphiphilic structure-directing agents. Another advantage is that high-temperature syntheses can be carried out when hard templates are used rather than soft templates [18].

Synthesis of hierarchically porous cobalt oxide (Co_3O_4), tin oxide (SnO_2), and manganese oxide (MnO_2 or Mn_2O_3) monoliths (average SSA 30–70 m^2/g) was carried out by this nano-casting route, in which macroporous silica monoliths with adjustable pore size in the 0.5–30-μm range and mesopores in the 3–30-nm range were used as molds. The silica monoliths, obtained by techniques based on phase separation, were impregnated with a metal salt solution, which was subsequently decomposed to a metal oxide (MO_x) by heat treatments to form a SiO_2/MO_x composite. Finally, the silica component was etched either with a NaOH or with a HF treatment, and metal oxide replicas having multi-modal pore hierarchy were obtained [63, 64]. This procedure was also applied to the preparation of porous carbon, employing a polymerizable solvent (furfuryl alcohol) as the carbon precursor [65–67].

Impregnation of polymeric foams

Preformed, high-SSA, mesoporous silica nanoparticles can be used in place of liquid precursors as the building blocks to coat macroporous polymeric foams via a "nano-tectonic approach" to obtain a component having higher-order architecture [68]. Polymeric foams with different compositions, pore sizes, and pore morphologies can be used as templates for the synthesis of large ceramics with tailored hierarchical porosity. These templates are inexpensive, highly versatile, and readily available. Among other polymeric foams, PU has been used commonly in this field, since it is widely available on the market with nearly unlimited variations of the cell size and amount of total porosity.

Lee et al. [69] published the first report concerning PU foams as large-scale templates for the preparation of micro–macroporous monoliths of ZSM-5, silicalite-1, and TS-1 foams with ramified macropores. PU-supported ZSM-5, silicalite, and TS-1 samples were utilized to produce zeolite self-supported foams having high SSA reaching the values of ~450 m^2/g [69–72]. PU foams were also coated with bimodal mesoporous particles (UVM-7 and MCM-41) to produce monolithic macrocellular silica foams with a trimodal pore system (small mesopores–large mesopores–macropores) upon mineralization and subsequent elimination of the organic template by calcination at 540 °C [73, 74]. Textural large mesopores and macropores in the 20–70-nm range had their origin in the inter-particle voids, and the small intra-particle mesopore system (2–3 nm in diameter) were due to the supramolecular templating effect of the copolymer used in the synthesis of UVM-7 particles, whereas macropores with a size of hundreds of micrometers derived from the polymeric template. Impregnation of a PU foam (pores in the 50–250-μm range) with a precursor solution containing TEOS and block copolymer Pluronic F127, followed by calcination at 600 °C, gave silica monoliths, which were used as transitional templates for the growth of monolithic carbon samples via infiltration and polymerization of furfuryl alcohol with a hierarchical macro–mesoporous structure [75].

Contrary to PU and PS, UF foams are hydrophilic, therefore can be used as templates for the growth of solids from polar solvents. Silica, zirconia, and titania were produced by a nanocasting approach by repeated impregnation of a UF foam followed by calcination, obtaining a meso–macroporous solid with mesopores of 3–4 nm [76]. One of the advantages claimed by the authors was that the hydrophilic nature of the UF foam enabled the use of polar, organic solvent-free precursors, making this synthesis a "green" one. Using the same type of polymeric template, high SSA (324 m^2/g) silica monoliths were produced having meso (~4.5 nm)- and macroporosity tunable below 5 μm, by changing the processing conditions for the production of the polymeric foam [77].

Large multimodal porous monoliths (small mesopores–large mesopores–macropores) with foam-like morphology were obtained using preformed silica mesoporous submicron- or nano-particles as building blocks, which were used to coat PU foams of different densities, followed by elimination of the organic foam by calcination [73]. The resulting porous structure presented highly ramified networks defining interconnected large macropores, with diameters ranging from hundreds of micrometers to millimeters. The size of the macropores and the wall thickness could be fine-tuned by the choice of the PU foam and by the number of impregnation treatments. Hierarchical macro–mesoporous γ-Al_2O_3 foams with highly ordered two-dimensional (2D) hexagonal crystalline mesoporous walls were also produced using a triblock copolymer P123 as the mesoporous structure-directing agents and PU foam as the macrotemplate [78].

Giunta et al. [79] obtained mesoporous silica monoliths containing oriented macroporous channels by the application of an electric field to a polyacrylamide hydrogel transitional template during polymerization and cross-linking. The polyacrylamide monolith was immersed in neat TMOS, which underwent hydrolysis and condensation reacting with water trapped in the voids, and the organic phase was then removed by calcination.

In Fig. 2, the morphology of components produced with some of the templating techniques described above is shown.

Biological templates

Compared to synthetic hard templates, the structures of biological materials are often "naturally" hierarchical, complex, and unique, in that their architecture differs from species to species even within the same genus. Biological templates can be used for the development of ceramic materials with innovative structures that cannot be obtained with synthetic templates. A library of biotemplates already exists [80], making it possible to synthesize materials with unique structures and morphologies either using these templates directly in the synthesis procedure, or using nature as a source of inspiration in materials chemistry [81, 82]. Biological templates are generally inexpensive, abundant, renewable, and environmentally benign [83, 84]. Natural complexes such as starch gel [85], wood [86, 87], plants [88, 89], palm fibers [90, 91], cuttlebone [92], diatoms [93–95], bacterial threads [96] have been used as templates to produce zeolite components with micro–macro porosity. The excellent strength and specific stiffness of these biomorphic ceramics open a wide range of applications for these attractive materials [80].

A limitation in the in situ growth of micro- or mesoporous materials in biological specimens is the incompatibility between the organic substrate and the inorganic precursors. This can be solved using silica-containing plants such as *Equisetum arvense*, which were transformed into ceramics with hierarchical porosity that retain the morphological features of the biotemplate [89]. Uniform abundant nucleation of zeolite in the volume of the plant tissues induced by the biomorphic silica provided faithful replication of the plant structure and very high concentration of zeolite per unit mass of the material. Another approach for overcoming this limitation is to assemble presynthesized microporous nanoparticles on the biological supports, in a process similar to petrification of biological cells. For example, seeds have been used to induce zeolite formation on fossilized silica shells of single-cell algae (diatoms) via either liquid [93] or vapor [94] phase transport, and infiltration of zeolite nanocrystals into the void spaces of bacterial threads resulted in micro–macroporous zeolite fibers [85, 97].

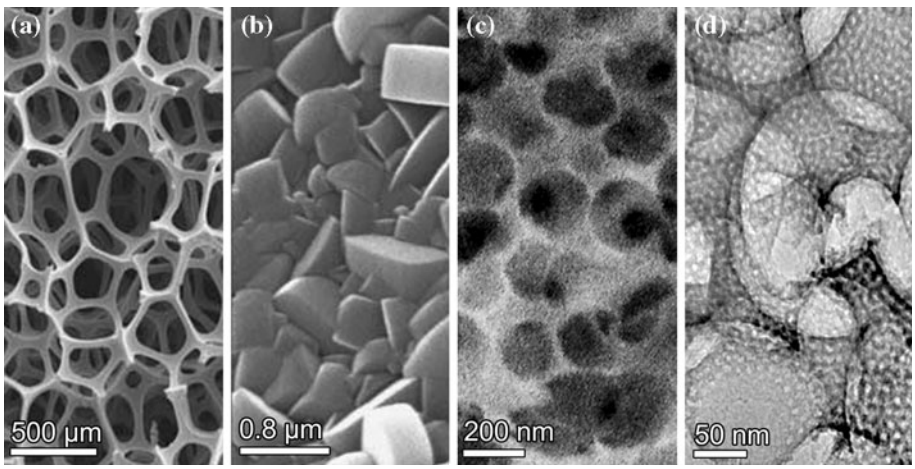

Fig. 2 **a** SEM image of a silicalite foam produced by templating with polyurethane foams; **b** strut detail upon reaction with synthesis gel for 8 h [70]; **c** SEM image of silica monolith produced by dual templating using both surfactants and colloidal PS spheres; **d** Bright-field TEM image of the same sample [54]

Templating strategies with natural materials can be extended to several compositions; e.g., Iwasaki et al. [98] prepared starch sponges with high internal macroporosity by freezing and thawing of starch gels. The sponges were then infiltrated with colloidal suspensions of titania nanoparticles and air-dried to produce TiO_2-starch foams with pores up to 200 μm, depending on the starch concentration and the TiO_2 loading, with the titania nanoparticles covering the surface of the sponges. No organic fragments remained in the TiO_2 sponge after heating at 600 °C for 2 h, and the produced foam had 65 m^2/g SSA, including meso (6.5 nm)–macro porosity. The TiO_2 sponges showed photocatalytic activity significantly larger than that of commercial materials. Compared with the freeze–thaw technique using inorganic templates, this process has the advantage of being facile, low-cost, environmentally benign, and amenable to scale-up.

Four kinds of wood templates were used for the growth of iron oxide with meso- and macropores, by sequential impregnation–calcination of a nitrate solution [99]. The microstructural features of wood ranged from millimeter (growth ring patterns) via micrometer (tracheidal cell patterns, macro- and microfibril cell wall textures) down to the nanometer scale (molecular cellulose fiber and membrane structures of cell walls) [100]. Thus, compared to other natural systems, wood could readily be used as a template to generate cellular ceramics with multi-modal pore hierarchy [83, 84, 101–103]. For instance, cellular β-SiC ceramics were synthesized at 1400 °C from pine wood infiltrated with silica gel [101]. The presence of both long cylindrically shaped macropores and slit-shaped mesopores was observed, with the formation of SiC whiskers with a diameter of 20–400 nm and a length of 5–20 μm inside the macropores; the material possessed an average SSA of $\sim$14 m^2/g. Mineralization of wood cellular structures using surfactant-templated sol–gel solutions has been investigated by Shin and co-workers [104]. The authors successfully prepared both positive and negative replicas of the wood by changing the pH values [105], and utilization of surfactants resulted in a high SSA samples (350–650 m^2/g), which is one order of magnitude larger than that of samples prepared without the use of surfactant (SSA < 45 m^2/g). The surfactant micellar structures incorporated in the silica network, which produced organized nanoporous channels during calcination, were found critical in maintaining the structural integrity, because they provided pathways for the release of gases generated by the decomposition of the organic part, without degradation of the whole structure. In another study [103], high SSA cellular SiC ceramics were obtained via carbothermal reduction of silica mineralized wood. It was reported that the synthesis using acidic conditions resulted in a ceramic with high SSA (60–100 m^2/g), where the pore sizes were randomly distributed from nanometers to micrometers, implying that a hierarchically ordered architecture with organized nanoporous channels within the cell walls was formed [106].

Emulsions

Owing to intense research in the last decades, colloidal dispersions can now be manipulated to induce ordered structures with limited number of defects [39, 106, 107]. However, when hard colloidal objects are used as the templating units, the maximum pore size that can be reached in ordered structures is limited to the colloidal dimensions, i.e., $\sim$1 μm. This can be a strong limitation in solids where diffusion of species is a critical requirement, such as in catalysis and in separation. Another disadvantage of using hard templates is that considerable shrinkage occurs upon drying, condensation, and densification of the templated ceramic structure, which can lead to cracking and pulverization [108]. The size limitation issue can be overcome by adopting templating strategies based on emulsion systems, which yield architectures structured on a scale ranging from $\sim$5 to 600 μm. These techniques lead to the fabrication of meso–macroporous silica foams based on the rearrangement of the inorganic precursors along the emulsion structure, which acts as a macroscopic "soft" scaffold. Furthermore, these templates can be readily removed by dissolution or evaporation after the templating stage and prior to densification and calcination. As an example, microemulsions have been used in mesoporous oxides to extend porosity beyond the limited pore size offered by amphiphilic block copolymers: ordered mesostructures of several tens of nanometers have been obtained by employing microemulsions from block copolymers and a cosolvent such as TMB, which acts as a micelle swelling agent [26, 109].

Emulsions consist of droplets of one fluid dispersed in a second immiscible fluid. According to droplet size, emulsions are classified into three groups, namely: macroemulsions (0.2-50 μm), mini-emulsions (0.1-0.4 μm), and micro-emulsions (0.01-0.1 μm) [110]. Whereas microemulsions are thermodynamically stable (due to the marked decrease in the size of the water droplets that form spontaneously upon mixing water, oil and a surfactant acting as a stabilizing agent) [111], macro- and mini-emulsions are unstable states which are usually produced by mechanically induced droplet breakup (kinetic stabilization) [108]. A direct consequence is that micro-emulsions are made of droplets of approximately the same size, whereas in macro- and mini-emulsions a distribution of droplet sizes is typically observed, though highly monodisperse droplets can still be generated [112]. If the volume fraction of monodisperse droplets is sufficiently high

(typically above 50 %) the droplets may spontaneously order to form a close-packed structure. When a ceramic precursor sol is added to the continuous (outer) phase of the monodisperse emulsion and its gelation is induced, for example by increasing the pH in the case of alkoxides, the structure freezes and porosity can be obtained upon condensation and removal of the organic phase. Macroporous titania, silica, and zirconia templated by highly monodisperse macroporous materials, with pore sizes ranging from 50 nm to several micrometers, were first reported by Imhof and Pine [113], who utilized emulsion droplets as the templates around which material was deposited through a sol–gel process.

If a structure-directing agent is added to the emulsion, mesopores can be generated, thus obtaining hierarchically porous materials. An advantage of the emulsion templating technique compared with hard templating is that, whereas samples prepared using rigid sphere templating tend to break into submillimeter-sized pieces, samples templated by emulsion droplets are deformable and are able to accommodate the stresses arising upon shrinkage during gelation.

An oil-in-formamide emulsion of water-sensitive TTIP in anhydrous formamide in the presence of a triblock copolymer, followed by hydrolysis and condensation of the alkoxide upon exposure to water, produced highly porous crystalline titania with a microstructure consisting of spherical shells ($\sim$10-μm diameter) with 0.12-μm thick mesoporous walls [114]. A similar strategy was adopted by Yi et al. [115]. Mesoporous titania particles with macroporous architecture were prepared from TTIP in the presence of a $C_{16}(EO)_{10}$ surfactant [116]. The structure was composed of a core with a sponge-like macroporous structure and a thick shell, characterized by an uniform pore size gradient decreasing from the core region (a few hundreds of micrometers) to the outer region (tens of nanometers). Compared with the hard templating approach, using mesostructure-directing agents in combination with emulsion has the advantage that the emulsion droplet size can be adjusted by changing the emulsification conditions. The use of block copolymer species, which self-assemble to a large extent independently of the emulsion formation, allows tailoring the macro- and mesopore size.

Inorganic condensation can be induced at the air–liquid interface in the process of air foaming. Bagshaw et al. [117] prepared silica and metallo-silicate materials possessing open macroporous skeletal networks of amorphous silica and templated mesoporosity within the solid skeleton. These hierarchical structures were formed from TEOS solubilized within the water-rich phase of metastable air–liquid foam stabilized by a PEO-based surfactant. The foam bubble sizes, and therefore the final macropore size, was modified by altering the mechanical shearing, i.e., turbulence within the reaction vessel; however, only a rough control could be obtained by variation of the stirring speed and use of magnetic stirring bars with different shape. Another bubbling process, developed by Carn et al. [118], allowed controlling the liquid fraction of the foam as well as fine tuning the macroporosity by adjusting the size of the pores in the glass disk employed in the bubbling process.

Hierarchical macro–mesoporous oxides can also be obtained in a two-step synthesis through a post-infiltration method. Monolithic PS foam was first obtained by polymerization of styrene either in the continuous or in the dispersed phase of highly concentrated W/O emulsions. In the second step, an inorganic precursor containing triblock copolymer Pluronic P123 was imbibed in the PS foam, which served as a scaffold for the condensation of the mesostructured oxide. The organic components were removed upon calcination or solvent extraction, and yielded a meso–macroporous silica monolith with cellular macropores (0.3–2 μm) with 0.2–0.5 μm cell windows of and highly ordered mesopores (5.1 nm) [119]. An advantage of this approach is that the structure-directing agents on two length scales (block copolymer and emulsion) do not interfere in the synthesis process, therefore optimization of meso- and macroscopic structure can be accomplished independently. Furthermore, the porous component can be molded into macroscopic 3D bulk shapes. An oil-in-water emulsion formed by mesytilene and TEOS added to a CTAB solution yielded a material characterized by 3D interconnected macropores having a strut-like structure, similar to meso-cellular silica foams, with wormlike mesoporous walls, and a very high SSA of $\sim$800 m^2/g with narrow mesopore size distribution [120, 121].

Carn et al. [122] prepared a macro–mesoporous monolith based on the arrangement of silica nano-building blocks along the confined geometry of an air–liquid foam structure, which acted as a macroscopic scaffold. Colloidal silica was prepared via the Stöber method [123], then a foaming solution was obtained by mixing concentrated colloidal silica and a cationic surfactant in an aqueous media at pH 9, and a foam was generated by continuous bubbling of perfluorohexane-saturated nitrogen through a porous glass disk. After 10 h of drying under ambient conditions and free drainage, a monolithic macroporous hybrid material was obtained and further thermal treatment at 650 °C led to a pure inorganic monolith. This method was demonstrated to lead to better control over the macropores characteristics, in particular size, topology (open- or closed-cell macrocellular networks) and morphology (spherical or polygonal cell structure).

Hierarchical macro–mesoporous metal oxides with funnel-like macroporous architecture were synthesized in a one-step procedure by single-surfactant templating. The

authors suggested that the single surfactant would direct the formation of inorganic phases with multidimensional pore systems by the formation of vesicle-type supermicelles, resulting from the aggregation of unreacted excess surfactants [124].

Phase separation techniques

A well-established technique to produce silica-based monolithic gels with multiscale porous structures makes use of the sol–gel process accompanied by phase separation. Nakanishi [125] produced monolithic silica with interconnected macropores and textural mesoporosity using the sol–gel process, in combination with a variety of water-soluble polymers to control phase separation and gelation kinetics. This process proceeds via formation of a gel from alkoxides in the presence of water-soluble organic polymers, such as PEO. Inorganic condensation occurs concurrently with spinodal decomposition, resulting in the formation of a bicontinuous gel, constituted by two interconnected SiO_2-rich and solvent-rich phases on the length scale of micrometers. This spinodal decomposition, with comparable volume fractions of the conjugate phases, typically exhibits a bicontinuous structure, where both the gel phase and the solvent phase are continuous and highly interconnected. When the onset of phase separation occurs at the point of sol–gel transition, the microstructure is frozen in as permanent morphology of the resultant gel. Subsequent solvent exchange with a basic solution and thermal treatment yields a structure in which macropores arise from the solvent-rich phase, and mesopores in the SiO_2-rich phase occur via a dissolution-reprecipitation (Ostwald ripening) mechanism, giving rise to textural mesoporosity with pore sizes in the 10–20-nm range and a high SSA. The macropore size can be controlled by adjusting the polymer concentration and can be varied nearly independently of the macropore sizes via a post-synthesis treatment in ammonia solution through partial dissolution and reprecipitation of the macroporous wet gel [126]. Following this route, hierarchically porous titanium [127, 128] and zirconium oxides [129] have been obtained, though formation an interconnected porosity was hindered by the high reactivity of transition metal alkoxides. Macroporous [130] and hierarchical bimodal structures [131, 132] allow transport of fluids in the macroporous interconnected cavities, so that these materials have been implemented in novel types of chromatographic columns without particle-packed structure, providing high efficiencies at high flow rates unlike conventional packed columns [133].

Smått et al. [134] adopted a phase separation–double templating approach, utilizing a cationic surfactant (CTAB) and a non-ionic polymer (PEG). The macropore diameter, which was mainly controlled via PEG/nanoparticle interactions, could be varied almost independently on the mesopore diameter through the incorporation of supramolecular CTAB aggregates, formed above the cmc by simultaneously varying the amounts of PEG and CTAB added in the sol. However, the pore organization did not exhibit mesoscopic long-range order.

Hüsing et al. [135] were probably the first to report the synthesis of hierarchical macro–mesoporous silica monoliths obtained by phase separation with ordered mesopore organization. An ethylene glycol-modified silane was used as the Si source instead of TEOS or TMOS, together with an amphiphilic triblock copolymer, followed by supercritical extraction with ethanol to remove the organic phase. The reason for a higher degree of mesopore order was that ethylene glycol was released during the hydrolysis and condensation reactions, instead of the short-chain alcohols (such as ethanol or methanol) which are produced when using TEOS or methyltriethoxysilane (MTES). In fact, contrary to short-chain alcohols, glycol does not disrupt the mesophase so it is not detrimental for most of the liquid crystal surfactant mesophases [136]. The pores in the macro- and mesopore size range possessed an extremely complex and finely detailed morphology. The use of 1,2-bis(trimethoxysilyl)ethane as the Si source and the introduction of TMB in the reaction mixture as the co-solvent significantly enhanced the degree of order of the mesostructure in monolithic hierarchical macro–mesoporous hybrid organic–inorganic ethanesilica [137]. The proposed explanation was the stabilization of the Pluronic P123 cylindrical micelles by TMB. Further additions of TMB induced additional structural transformation from 2D-hexagonal, through possibly 3D-hexagonal, to MCF, with relatively narrow pore size distribution. Pure inorganic silica monoliths having a hierarchical pore structure, with both well-defined bicontinuous macropores and highly ordered mesopores, were also obtained [138]. The use of glycol-modified silanes in combination with a non-ionic block copolymer surfactant allowed the formation of monolithic, 3D gels with a hierarchical network structure and an interconnected, multilevel pore system with highly ordered mesophases [139]. A silica monolith with interconnected macropores, textural pores, and ordered mesopores was fabricated in the presence of block copolymer Pluronic F127, which acted both as a phase separation inducing agent and as a mesostructure-directing agent [140]. Triblock copolymer Pluronic P123 was used both as the structure-directing agent and as the phase-separation inducer in the synthesis of a macro–mesoporous silica monolith with interconnected macropore and mesopores. This monolith was tested in a chromatographic column, showing fast separation rate with low back-pressure for the separation of benzene and phenol [141].

Backlund et al. [142] have proposed an interesting sol–gel approach for a direct, template-free, synthesis of titania monoliths exhibiting a hierarchical, bimodal meso-macroporosity (SSA < 180 m^2/g, macropores < 4 μm, and mesopores in the 3–4-nm range). Because this synthesis is carried out from simple and relatively cheap chemicals, such as titanium isopropoxide, HCl, and acetic acid, it is straightforward and convenient from an economic and environmental point of view. The macropores form as a consequence of parallel gelation and microscopic phase separation, in which their relative kinetics determines the macropore diameter. The macropore diameter can be varied in the range 0.4–4 μm by controlling the concentration of acetic acid, which acts as a titania chelating agent, whereas the mesoporosity is formed as interparticulate porosity upon crystallization of the amorphous TiO_2 into anatase.

Other templating routes

Freeze-casting enables templating porous structures by the solidification of a solvent, and is gaining significant attention for the fabrication of components with complex, multi-scale morphology [143]. In fact, ice crystals can be used as macrotemplates, as demonstrated by Nishihara et al. [144, 145] who prepared ordered macroporous materials with micro–mesoporosity by thermal-induced phase separation. By this method, it is possible to precisely control the macroporosity, wall thickness, and micro/mesoporosity of silica materials via extremely simple procedures. When compared with conventional methods, the ice-templating method has many advantages, such as: flawless components with monolithic shape can be produced, it does not require the addition of special templates which usually lead to high production costs and require severe removal processes (e.g., calcination and chemical etching, using a strong base). For example, macroporous monoliths of SiO_2–Al_2O_3 cryogels were prepared by ice-templating of mixed metal oxide hydrogels of SiO_2–Al_2O_3, which were synthesized by the sol–gel technique. Unique shapes, such as macroporous monoliths with interconnected macropores and fibers, were formed and nitrogen adsorption–desorption measurements indicated that the macroporous walls were micro/mesoporous with high BET surface area (700 m^2/g) and large pore volumes (0.45 cm^3/g) [146].

Hybrid techniques have also been used to synthesize hierarchical porous ceramics. For example, hierarchical 3D porous bioactive glass scaffolds with highly ordered mesoporous structures were prepared using a combination of rapid prototyping and templating [147]. The scaffold contained three types of pores: mesopores (5.4 nm) templated by block copolymer (Pluronic F127), macropores (10-100 μm) produced using a methyl cellulose template, and large pores (>100 μm) produced by the rapid prototyping technique. In vitro tests demonstrated bone-forming bioactivity of the porous scaffold: apatite formed on the surface of the bioglass scaffold upon soaking in simulated body fluid for 24 h; this hydroxyapatite-like phase was composed of rod-like particles with a length of around 100 nm, similar to the morphology of hydroxyapatite in human bones.

Ocampo et al. [148], starting from glass monoliths having meso- and macropores, introduced additional microporosity exploiting the growth of zeolite crystals via partial recrystallization of the glass support into ZSM-5 zeolite phase. The starting monolith exhibited three pore families in bimodal length scale (macro–meso), with macropores around 300-500 μm produced by rapid prototyping, macropores around 10-100 μm using a methyl cellulose template, and mesopores of 4-5 nm with 2D hexagonal pore structure produced by P123 triblock copolymer self-assembly. Structured zeolitic catalytic materials were then grown on the glass support by conventional self-assembly of template cations and silica species. These zeolite/glass composites exhibited enhanced diffusional properties in comparison with purely microporous zeolite materials and were tested as a catalyst, demonstrating high activity, when compared to commercial catalysts, in *n*-hexane cracking (chosen as a model acid-catalyzed reaction), together with higher selectivity toward C_2–C_3 light olefins.

Powder processing routes

The preparation of hierarchically porous ceramics components requires control of the pore architecture, especially as far as size, size distribution, morphology, and 3D connectivity are concerned, and different synthetic pathways can be adopted to precisely tailor porosity. However, another important requisite for several advanced applications such as high-performance chromatography [133, 149], microreactors [150], and environmental applications [9] is the possibility to form a well-defined macroscopic shape with satisfactory mechanical properties. Ceramic-forming techniques such as pressing, extrusion, tape casting, slip-casting, and gel-casting are versatile processes that can be successfully applied to shape porous ceramics. For example, El Haskouri et al. [151] showed that casting or extrusion techniques applied to mesostructured nanoparticles enabled the fabrication of mesoporous monoliths (with a size of several centimeters) possessing disordered bimodal pore structure; however, the authors did not disclose the preparation details and the mechanical properties were not measured.

Hierarchical zeolite structures with well-controlled microstructures and complex-shaped ceramic bodies were

obtained by gel-casting of zeolite nanocrystals, such as silicalite, ZSM-5, TS-1, Beta, A, and FAU using a polyacrylamide hydrogel [152]. The products had a typical BET surface area of 516 m^2/g and three-level porosities including sub-micron macropores, mesopores (16–13 nm), and micropores (0.55 nm).

Shape forming of ceramics was recently done by a drying-free colloidal casting method. Furfuryl alcohol was used as a polymerizable solvent to disperse ceramic particles (e.g., NiO/YSZ, Al_2O_3, and YSZ) and then polymerized into poly(furfuryl alcohol) to bind ceramic particles together. The slurry was shaped into different forms by casting or coating and then treated at 70 °C for 2-10 h for furfuryl alcohol polymerization and suspension solidification. The resulting ceramic green bodies were sintered at 1350-1450 °C for 2–5 h. The poly(furfuryl alcohol) contained in the ceramic green bodies acted as a molecular porogen for formation of porous ceramics [153].

HPLC monolithic silica columns with defined mesopore and a tunable macropore structure were fabricated by gel casting of ordered mesoporous silica precursors [154]. Mesoporous silica particles (MCM-41, MCM-48, SBA-15, SBA-16, and HMS) were enclosed in a cross-linked polyacrylamide macromolecular gel, which replicated the shape of the mesoporous model. A glass tube was then packed with the gel, polymerized into an elastic hydrogel and sintered at 700 °C for 10 h. The monoliths (3.8-mm internal diameter with lengths ranging from 5 to 25 cm) were then chemically bonded to a stainless steel tube via a TFE interlayer and tested as HPLC columns, showing good resolution with extremely low hydraulic resistance and rapid separations. Both the macropores and the mesopore modes could be adjusted, thus tailoring the hydraulic resistance of the column.

In conventional (pressureless) sintering, the mass transport at the contact points that is necessary to form the solid necks providing the strength of the material is thermodynamically driven by the minimization of surface free energy. Therefore, a competition between the reduction of the internal and the external surface areas can either result in a mechanically stable monolith but compromise the internal pore structure, or preserve the internal porosity but produce a weakly bonded monolith [154]. Hierarchically porous ceramic monoliths have been fabricated by PCP. The rapid temperature increase, which is created by an electrical current that is passed through the die, associated with the application of pressure, enables the formation of necks between micro/mesoporous particles, without the elimination of internal porosity due to limited mass transport. Mechanically stable hierarchically porous silica monoliths, with tunable open macropores and surfactant-templated ordered mesopores, were fabricated by PCP [155]. Rapid heating (up to 750 °C) of mesoporous powder assemblies, produced by an aerosol-assisted technique, were subjected to a compressive stress resulting in viscoelastic deformation and partial fusion of the mesoporous silica particles at the contact points. This process produced monoliths with a bimodal porosity, in which the original mesopore size was retained. The products could be shaped by either using dies of various geometries or simple machining. Diatomite powders have also been processed using PCP leading to hierarchically (macro–macro) porous ceramic monoliths in which the powders were bonded together without significantly destroying the internal pores of the diatomite powder, at a temperature range of 700–750 °C [156]. Little fusion at the particle contact points occurred at temperatures below 650 °C, whereas the partial melting and collapse of both the interparticle pores and the internal structure occurred at temperatures above 800 °C.

Another recent study in this field was performed in our laboratory using SiOC PMO particles [157]. SiOC monoliths possessing hierarchical porosity were produced via a one-pot processing method, in which PMO particles were embedded into a foamed polysiloxane preceramic polymer. After pyrolysis at 1000 °C in inert atmosphere, SiOC ceramic monoliths with a high amount of interconnected open cells, ranging in size from several to hundreds of micrometers, were obtained. The components possessed a SSA of 137 m^2/g, indicating the retention of most of the mesopores after the pyrolytic conversion of the PMO precursor particles, which were homogeneously distributed throughout the SiOC cellular matrix.

In Fig. 3, the morphology of components produced with some of the powder processing techniques described above, corresponding to the passage from micro- and mesoporosity to monoliths possessing multiscale pore hierarchy, is shown.

From macroporosity to multiscale pore hierarchy

A macroporous monolith can serve as a host matrix, to which micro- and/or mesopores are then added using different strategies. By the term "macroporous monolith," we mean a porous ceramic that exhibits a total porosity higher than ~60 vol% (i.e., specifically a cellular ceramic) with an average cell size of the order of several microns to a few millimeters. Cellular ceramics constitute a specific class of materials containing a high level of porosity which are characterized by the presence of a recognizable "cell," that is an enclosed empty space possessing faces (cell walls) and solid edges (struts). For the production of components with hierarchical porosity, it is necessary that openings (cell windows) are present in the cell walls and therefore the cells are interconnected. The structure of a cellular

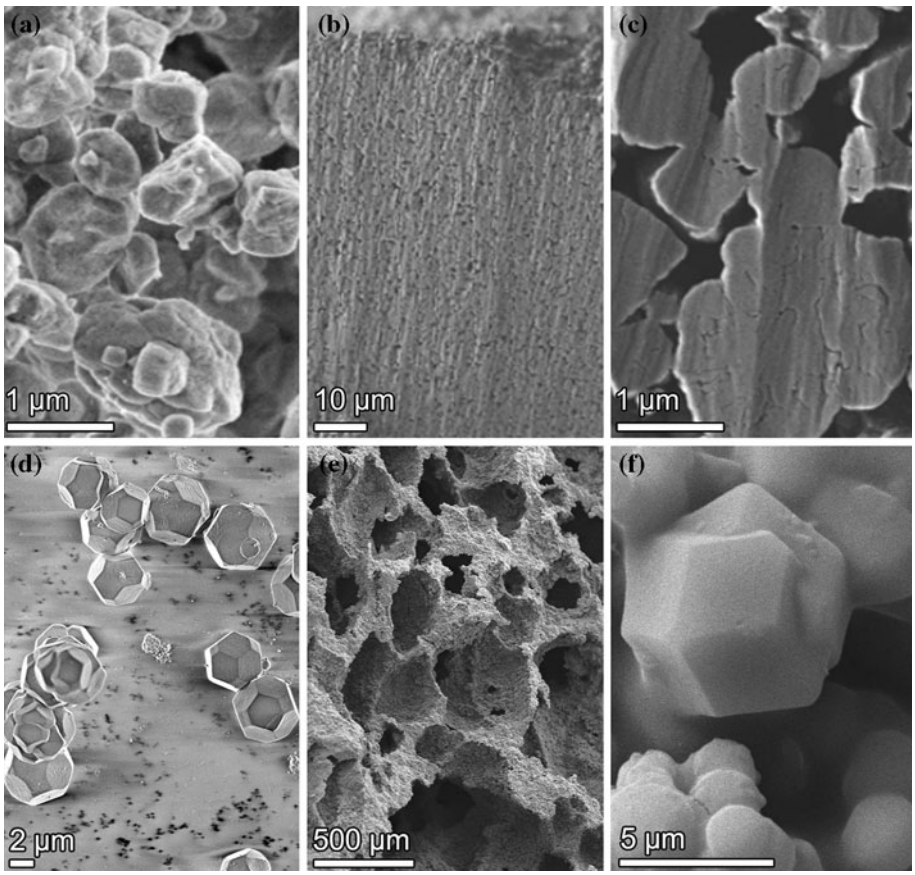

Fig. 3 **a** SEM image of as-received ZSM-5 powder; **b** SEM image showing the overview of the polished section of the monolith; **c** polished cross section surface of a monolith produced by PCP at 1200 °C (images courtesy of P. Vasiliev and L. Bergstrom, NeoZeo AB and Stockholm University, Sweden); **d** FEG-SEM image of PMO particles (pyrolyzed at 1000 °C); **e** SEM image of the fracture surface of SiOC foam containing PMO particles (pyrolyzed at 1000 °C); **f** detail of a cell wall showing the truncated rhombic dodecahedral shape of an embedded PMO particle

ceramic consists of polyhedral cells that are arranged three-dimensionally to efficiently fill the space and, depending on the overall morphology, a structure typical of a honeycomb (possessing parallel prismatic cells) or of a foam (for which cell walls are randomly oriented in space) can be identified [158, 159]. In addition to this, cells can be regular or exhibit random or graded variations in size, shape and distribution, thus further extending the range of morphologies that cellular materials can exhibit. Besides foams and honeycombs, connected rods, connected fibers, connected hollow spheres, and components obtained from the replica of biological templates are also examples of cellular structures that are being produced nowadays. It should be noted that cellular ceramics typically posses low SSA values (<2 m^2/g), and thus adding smaller length scale pores to the macroporous network results in an increase in SSA of the cellular component.

Thanks to their structure, cellular ceramics display a rather unique combination of properties, such as low density, low thermal conductivity, low dielectric constant, low thermal mass, high specific strength, high permeability, high thermal shock resistance, high porosity, high geometric surface area, high wear resistance, high resistance to chemical corrosion, and high tortuosity of flow paths, making them indispensable for various engineering applications [15, 16, 160, 161].

Processing strategies to add micro- and/or mesopores, or high SSA, to a cellular ceramic include coating (deposition of thin continuous films or surface attachment of discrete micro/mesoporous particles), growth of one-dimensional (1D) nanostructures (nanofibers, nanowires or nanotubes), selective etching, full infiltration with a micro/mesoporous material, or the exploitation of the inherent characteristics of preceramic polymers (Fig. 4).

Coating

Coating the cell wall surface of a macroporous ceramic with a high SSA layer is a well-established route, which has been widely used to fulfill the specific requirements of industrial applications (such as catalytic converters in automobile industry) for several decades. In particular, the

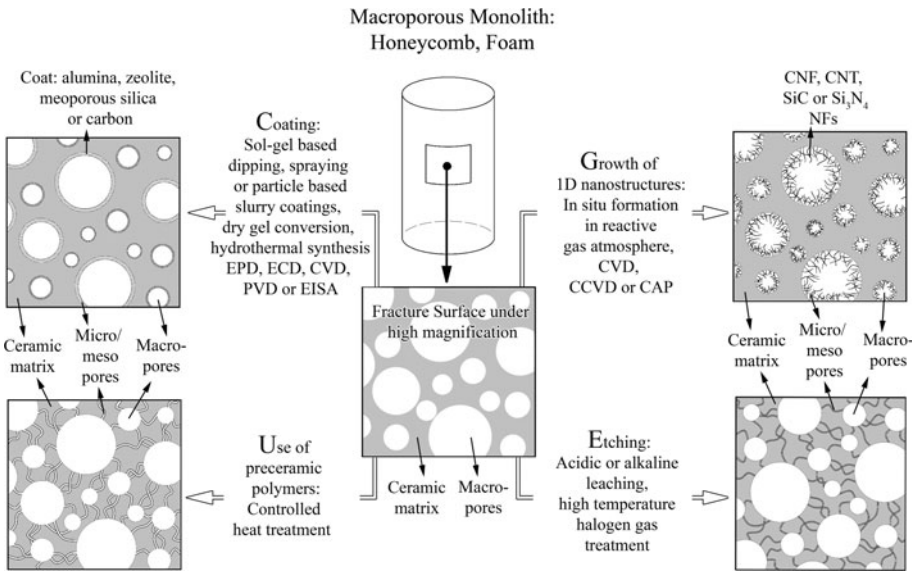

Fig. 4 Fabrication of ceramic components with hierarchical porosity. Processing strategies for adding micro/mesoporosity to macroporous materials

high geometric surface area (of the order of a tens of cm^2/cm^3 to a few m^2/cm^3) of cellular materials provides a wide region for the deposition of coatings possessing micro/mesoporosity, and the complete interconnection among the cells supplies easy access to the coating solution or slurry. In principle, any high SSA material can be used as a material for coating/deposition on macroporous cellular ceramics, provided that the introduction of this secondary phase maintains the permeability of the structure. Typically, this approach leads to components having bimodal porosity (micro/macro or meso/macro), with only a few examples of trimodal pore architecture. The thickness of the deposited layer (commonly termed a "washcoat") is a parameter which strongly influences the final SSA value of the component, as well as other characteristics (such as adhesion, scratch resistance, catalyst loading, etc.), and it depends on the deposition technique (which range from solution-based dipping and spraying to slurry coating, electrophoretic or electrochemical deposition, chemical or physical vapor deposition) [9, 162–165]. For example, the sol–gel method typically allows to form <10-μm thick layers, whereas by vapor deposition methods layers thinner than 1 μm are typically obtained, and suspension-based methods lead to layers with a thickness ranging from ~1 to ~100 μm. As some reviews have already comprehensively illustrated the different coating methods [9, 162–165], we will here focus mainly on the type of material that is deposited on the macroporous substrate.

Analogous to anodic oxidation, which is generally applied to aluminum structures to obtain a porous alumina layer at the surface [162], γ-Al_2O_3 (SSA ~ 200 m^2/g) is commonly used as a coating material for cellular ceramics. This material, deposited on several substrates (foams, honeycombs and ceramic fibers, all typically made of α-Al_2O_3, cordierite, zirconia, or silicon carbide) using several methods, [9, 162, 163, 166–168] increases the SSA of the porous body [2, 163, 169] and the structure remains stable up to temperatures of ~700–800 °C [170]. Typically, a dilute slurry containing the washcoat precursors (particle/colloidal suspension or sol with binders and small amounts of viscosity-modifying agents) is deposited on the substrate, which is then dried and calcined at moderate

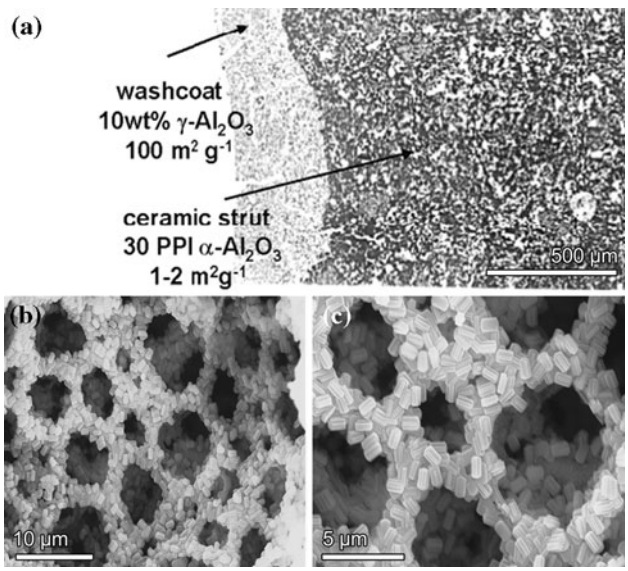

Fig. 5 **a** Backscattered electron image of a γ-Al_2O_3 washcoated ceramic foam strut [2]; **b** SEM image of a microcellular SiOC foam coated with in situ synthesized silicalite-1 zeolites; **c** detail of a group of cells [220]

temperatures (~500 °C) [163]. Using a suspension, thicker layers can be produced than by sol–gel [162], although repeating the solution coating procedure leads to an increase in coating thickness and SSA value (for example SSA of α-Al_2O_3 foam (~1 m^2/g) can be increased linearly with the γ-Al_2O_3 (SSA ~ 205 m^2/g) washcoat allowing to reach final values of ~35 m^2/g with repeated coating cycles giving a loading of 17 wt%, see Fig. 5a) [2]. The final characteristics of a washcoat are a complex function of the slurry properties: nature and particle size the precursor powder, loading amount, nature and concentration of dispersants, temperature of the slurry, and the presence of binders in the slurry [169–172].

Although coating of porous ceramic monoliths by γ-Al_2O_3 is well established, and improvements in processing methods have led to an increase in SSA up to ~45 m^2/g (starting from a low SSA ~1 m^2/g support) [2, 172–176] the final pore characteristics of the coated cellular monolith is scarcely documented, probably because the aim of most studies is simply to obtain a moderate-to-high SSA value (~20–60 m^2/g) or simply a rough surface, and not to produce hierarchical porosity. The pore nature (micro- or meso-) of the alumina washcoat is anyway shown to be dictated by the processing and especially by the type of the precursor used to synthesize precursor powders [177]. Agrafiotis et al. [169, 170, 178–180] studied the effect of powder characteristics and processing parameters on the properties of various washcoats such as alumina, zirconia, and titania for ceramic honeycombs. Using a sol prepared with a dispersible commercial colloidal pseudo-bohemite (γ-AlOOH) powder, they formed a mesoporous (mean pore size ~ 7.0 nm) γ-Al_2O_3 coating on cellular cordierite honeycombs (400 cpsi) [169]. Jarrah et al. [173, 174] also mentioned mesoporous alumina coatings possessing pores of 5–20 nm, deposited on 600 cpsi cordierite monoliths.

An alternative coating material commonly used is zeolite. Pure zeolite has a SSA in the range of 400–600 m^2/g [181] and a regular internal channel structure with pores <2 nm; therefore a monolayer of zeolite may satisfy the need for SSA requirements for many applications such as adsorbents, catalysts, and pollution abatement [182]. Strategies for the preparation of zeolite layers and membranes (thin films) on different substrates have been reviewed comprehensively [183, 184]. In general, zeolite coatings on cellular ceramic (and in most cases for all types of substrates) can be produced either by in situ crystallization through wet hydrothermal methods (direct synthesis, seeded growth—also termed secondary growth) or through vapor phase synthesis (dry gel conversion), or by depositing an existing zeolite phase as slurry (having either large single crystals or small crystallites) on the support [9]. The direct hydrothermal synthesis of zeolite crystals on ceramic surfaces is performed by prolonged contact of a cellular body with an aged zeolite gel inside an autoclave, and heating according to a precisely defined schedule. In the case of the dry gel conversion method, a sol or sol-containing template is deposited on the substrate, dried and treated with vapors of a template to form a zeolite layer. In the secondary growth procedure zeolite nanoparticles are seeded on a substrate and grown to a continuous thin film by hydrothermal synthesis [165, 185]. These synthesis methods have the advantage of achieving a stronger adhesion without the use of any binder, and the possibility of controlling crystal orientation [9] but, on the other hand, they are considerably more complex than slurry-coating and can hinder diffusion if a dense layer is formed [186–188]. Some recent publications have however shown the possibility of overcoming this problem [189, 190]. Utilization of zeolite crystals by a slurry-coating technique results in a coating consisting of randomly oriented zeolite crystal layers, useful for adsorption and catalysis purposes [162]. Slurry coating usually involves the addition of a binder material to the zeolite slurry to obtain a strong adherent coating. However, the binder (colloidal particles such as silica), which has mostly smaller crystals than the zeolite, may block the access to the micropores by surrounding the zeolite crystals [165]. Fortunately, it has been reported that the use of a binder is not essential for washcoating using zeolite powders with small particle size [165, 191].

These processing strategies have been used to create coatings of various zeolites (silicalite-1, HZSM-5, ZSM-5, mordenite, and Zeolite Y, etc.) on the surface of different cellular ceramics [165, 186–188, 191–213]. The SSA value of the final component, which is a consequence mostly of the microporosity of the zeolite crystals, depends on the intercrystalline porosity, the orientation of the zeolite crystals with respect to the support, the uniformity and degree of coverage ($g_{zeolite}/m^2$ support surface) and the thickness of the coating [198]. Excluding the studies quoted in the recent reviews of Meille [162] and Avila et al. [9] and focusing only on studies concerning zeolite coatings on cellular ceramics, we can state that most of the work in this field has been devoted to coat commercial cordierite honeycombs (200–600 cpsi), for several industrial applications. Components with SSA values up to ~100 m^2/g and high mechanical integrity have been produced, employing several coating approaches. Zeolite-coated honeycombs have been shown to possess higher mechanical integrity than monolithic bodies produced by extrusion of zeolites [57]. By in situ hydrothermal method, without organic templates, deposition of several zeolites types (ZSM-5, Linde A, Linde Y, and mordenite) on cordierite supports has been demonstrated [186, 192–197]. Mullite honeycombs have also been coated by a continuous ZSM-5 film (150–200-μm thick) by hydrothermal synthesis, and the

final component had a hierarchical pore architecture with micropores (0.5 nm in diameter) and macropores (0.5–0.6 mm) and high SSA (~90 m^2/g) [208]. The preparation of a continuous monocrystal zeolite thin film on cordierite honeycombs via in situ crystallization was also reported by Madhusoodana et al. [188] and other authors [193–195]. In a different way, slurry coating was applied by Beers et al. [209], Zamaro et al. [187], and later by Mitra and Kunzru [164] to produce a coat layer on cellular cordierite monoliths with various types of zeolites, including mordenite, ZSM-5, β zeolite, Zeolite Y, BEA (generally wet ball-milled to 2–3-μm size), leading to a significant increase in SSA in the final component.

Ceramic foams are used commercially for the filtration of molten metal, and are attracting increasing attention as catalyst supports due to their high thermal stability, high porosity, and increased tortuosity with respect to honeycombs. Also, foams are superior over particle-based beds from the viewpoint of combined high mass transfer and low-pressure drop [212]. Seijger et al. [199] studied hydrothermal synthesis of ZSM-5 zeolite coatings on α-Al_2O_3, SiC/Al_2O_3, and ZrO_2/Y_2O_3 foam supports (cell size ~0.04–1.5 mm and porosity ~80–90 vol%), and demonstrated that SSA of ceramic foams can be increased from <1 to >200 m^2/g by the in situ formation of 5–10-μm size zeolite crystals. Other authors used a seed-film method to produce zeolite thin coatings on ceramic foams, and documented the resulting increase in SSA values [192, 200]. Buciuman et al. [165] demonstrated the possibility to coat and enhance the SSA of ceramic foams (alumina–mullite, china, cordierite, or steatite, 10–80 ppi) without binder addition by simply dipping the ceramic body in an aqueous suspension of zeolite (silicalite—particle size 100 nm and HZSM-5—particle size 650 nm). Patcas et al. [213] used 500-nm size ZSM-5 particles to washcoat mullite-bonded alumina foams (45 ppi) and showed the formation of a bimodal pore size distribution. In a very recent modified washcoating approach, cordierite foams (porosity ~ 80 vol%) were coated with ZSM-5 zeolites after treating the surface of ceramic foams with an aqueous cationic polymer solution, which increased significantly the amount of zeolite loading in the final component [191].

In most of these aforementioned studies, the ceramic cellular support is considered to be inert under zeolite synthesis conditions, although high pH present during synthesis [165, 198, 199] can lead both to the deterioration of the support and a modification of the gel composition [188, 214, 215]. This feature has however been exploited in a novel approach, which utilizes the partial dissolution of the substrate to supply Si or Al atoms needed for the in situ formation of zeolites. A significant advantage of this approach is a higher degree of adhesion to the substrate, reduced difference in coefficient of thermal expansion between substrate and coating, and high zeolite loading. Crystallization of zeolites on other cellular supports has been reported, including porous glasses [216, 217], SiC [214, 215], or polymer-derived-ceramic foams [218–220] and biologically derived substrates. In the case of biologically derived substrates [102, 221], micro–meso–macroporous components were produced (tri-modal pore hierarchy). Preceramic polymer-derived microcellular foams were also used as reactive substrate for the formation of Silicalite-1 and ZSM-5 zeolites layers, giving high SSA (~342 m^2/g) and a relatively strong component possessing hierarchical porosity (mean cell size ~ 8 μm, porosity ~ 84 vol%; compression strength 1–4.4 MPa) and high thermal stability (600 °C, air), see Fig. 5b and c for the SEM images of the produced components [220]. Tong et al. [222] prepared zeolite beta monoliths with a trimodal pore structure of interconnected macro-, meso- and micropores via the transformation of the amorphous silica walls of a macroporous component, using carbon as a transitional template to prevent the pore channels of the silica monolith from collapsing during conversion to zeolite beta. Similarly, Lei et al. [223] synthesized hierarchically structured monolithic silicalite-1 by transforming the skeleton of a macroporous silica gel into silicalite-1 crystals through steam-assisted conversion, followed by layer by layer coating [224]. Ocampo et al. [148], starting from glass monoliths having meso- and macropores, introduced an additional microporosity by allowing the growth of zeolite crystals via partial recrystallization of the glass support into ZSM-5 zeolite phase. Produced components showed high SSA (400–450 m^2/g) with hierarchically (tri-modal) porosity and hence, exhibited enhanced diffusional properties in comparison with purely microporous zeolite materials. These elevated mass transport properties allowed improvement of the selectivity toward light olefins in the important *n*-hexane cracking reaction. In a slightly different approach Ivanova et al. [215] observed for the first time the self-assembly of zeolite nanocrystals into fibers and thin films via in situ SiC support self-transformation. The SSA increased from 19 m^2/g for the pure β-SiC foam support to 55 m^2/g for the zeolite/β-SiC composite. This increase in SSA was connected with the generation of microporosity, which was absent in the pure β-SiC foam support, but is typical of zeolite-type materials. All the coating methods described above deposit zeolites covering the cell surface of a macroporous ceramic support, resulting in a porous monolith with hierarchical porosity (typically micro–macro; rarely micro–meso–macro). However, coating routes generally result in a composite ceramic which suffers from a low zeolite-to-support weight ratio, single-sided mass transport to and from the layers, and probable loss of zeolite layer from the supports upon repeated heating due to the difference in the thermal

expansion coefficients of the components, namely zeolite and substrate material [69].

An alternative coating material is mesoporous silica. Mesoporous MCM-41-like molecular sieves (M41S) [27] are very useful in applications where pore sizes larger than those typical of zeolites (micropores) are required [225]. Only one study focused on the use of pre-formed mesoporous silica nanoparticles as coating particles [225]; the authors produced a multiphase (silica-rich glass with mullite and quartz) foam using the replica technique, and then deposited UVM-7 mesoporous particles by multiple impregnations in a slurry. The stabilization of the particles on the ceramic surface was achieved by a low temperature treatment (120 °C), leading to a component with 229 m^2/g SSA, high coverage values (~17 wt%) and good compression strength (3–4 MPa). However, every impregnation cycle caused a decrease in the macropore diameter and, after five dip-coating cycles, blockage of the macropores. In a different approach, which does not require the pre-formation of particles, Costacurta et al. [226] prepared microcellular SiOC foams, which were shown to have good mechanical properties and high chemical durability, and deposited a mesoporous silica coating via EISA using a TEOS solution containing block copolymer Pluronic F127 as structure-directing agent. After calcination at 350 °C, the cell walls were uniformly covered by a highly ordered mesoporous silica layer (BCC unit cell) with a thickness ranging from <1 to ~5 μm, thus producing a meso–macroporous component with a SSA of 60 m^2/g (see Fig. 6a for the SEM micrograph of a macroporous SiOC foam coated with mesoporous silica, and Fig. 6b for the cross-sectional TEM image showing the ordered pore arrangement of the coating). Very recently, alumina-based macroporous ceramic foams were also successfully coated with MCM-41 mesoporous particles using an in situ one step hydrothermal synthesis, leading to monoliths having SSA values up to ~57 m^2/g [227].

Carbon coatings have also been deposited on cellular ceramic substrates to enhance SSA while obtaining hierarchical porosity; the tunable porosity and chemical surface properties of carbon coatings permit to adjust the characteristic of the coating for specific applications [228]. Carbon-coated ceramic honeycombs (clay containing [231], cordierite [232–247], and acicular mullite [248])

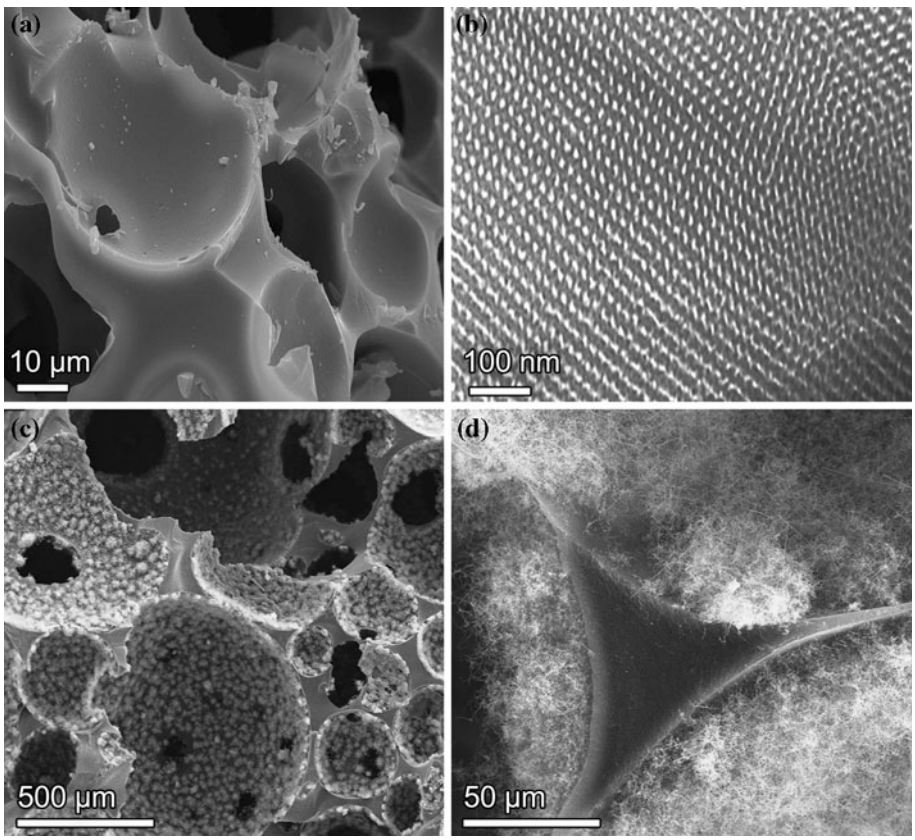

Fig. 6 **a** SEM image of a macroporous SiOC foam coated with mesoporous silica obtained via EISA; **b** cross-sectional TEM image showing the ordered pore arrangement of the mesoporous coating (courtesy of J. Woltersdorf, MPI Halle, Germany); **c** SEM images taken from the fracture surface of a macrocellular SiOC foam (pyrolyzed at 1350 °C, with Co catalyst), showing Si_3N_4 nanowires coating the cell walls; **d** higher magnification image showing a dense strut and nanowires protruding from the cell walls

and foams (commercial zirconia [249], alumina [250], and cordierite [251]) have been produced. In a typical process, these cellular ceramic supports are coated with a polymer solution (such as novolak, furan, etc.), dried and then heated at high temperature (500–1000 °C) in inert atmosphere to produce a porous carbon layer [228]. These coatings have been shown to enhance SSA and mechanical strength of the cellular substrates [233, 245, 250]. The carbon layer typically contains microporosity, but the presence of carbon accumulations forming spherical particles induces also a meso–macro porosity [250]. By the activation of the carbon layer (for instance by heating for 4 h at 900 °C in CO_2) very high SSA values up ~1400–1600 m^2/g can be obtained for the coat layer [233, 249]. It is worth mentioning that the surface area and porosity of carbon-based cellular materials controlled the adsorptive properties and dispersion of the catalysts. An alternative method to obtain carbon-based cellular structures is to add the carbon precursor, such as organic resins and polymers, to the dough to be extruded; details for these strategies can be found in the relevant literature [9, 228–230].

Growth of 1D nanostructures

Despite the fact that, strictly speaking, the presence of 1D nanostructures does not add porosity to a dense material, it is appropriate to discuss their growth on the surface of macroporous ceramics in the context of this review, as it has been demonstrated that their presence leads to an increase of the SSA of a component, therefore enabling it to fulfill similar applications than those of a properly termed hierarchical porosity monolith. Moreover, this approach allows producing alternative phases in the material, which can further functionalize the system (for example altering its mechanical, magnetic or electrical properties). A pioneering work in this field was reported by Jarrah et al. [173, 174], in which cordierite honeycombs (600 cpsi) were washcoated with a γ-alumina layer (enhancing the SSA from <1 m^2/g to values of ~25–45 m^2/g, depending on the layer thickness). Nickel was then deposited on the honeycombs and samples were heated in a reactive gas mixture (CH_4 or C_2H_4), leading to the formation of ~1-μm thick layer of CNFs (diameter of 10–30 nm) which caused an increase of the surface area of the cellular substrates up to 63 m^2/g [174]. The nanofiber diameter was controlled by the size of the deposited Ni particle, by the reactivity of the gas used over this particle, and by the duration of thermal treatment. This parameter, together with the total amount of nanofibers formed, strongly affected the final SSA of the component [173]. The total porosity decreased with the amount of CNFs, whereas the surface area per gram of monolith increased. BET analysis showed the presence of micropores, which were attributed to the space between the nanofibers and the pore walls of washcoat layer, and therefore not to the presence of pores in the substrate or washcoat layer which was previously characterized as mesoporous (pore size 5–20 nm) before CNF formation [173]. de Lathouder et al. [246–248] followed the same strategy using both silica-coated cordierite and alumina-coated highly porous acicular mullite honeycombs (200/400 cpsi). The authors demonstrated that CNFs-containing cordierite monoliths had ~8-nm mesopores which were again attributed to the space among the nanofibers and therefore not to the presence of pores in the substrate, resulting in a high enzyme activity for the CNFs-containing cellular ceramics. A direct correlation between nanofiber diameter and surface area was found, with a decrease in SSA occurring with increasing nanofiber diameter [247]. Further improvements by García-Bordeje et al. [251], using a thin (~0.1 μm) alumina washcoat, which prevented CNFs from being trapped inside its pores, led to the increase of the CNFs layer to ~4 μm. The authors underlined the significant influence of the nanofiber diameter and degree of entanglement on the morphology (density and uniformity) of the formed layer and resulting SSA of the porous components [252]. Interestingly, they showed also that the mechanical strength of the cordierite honeycomb (crushing strength of un-coated cordierite monolith was 22 MPa, 400 cpsi) was affected, with higher strength (30–35 MPa) achieved for a stronger adhesion of the CNFs layer to the substrate. A similar strategy was followed very recently, and it was shown that the surface area significantly increased with the CNF coating [253].

Ulla et al. [254] more recently studied the catalytic decomposition of C_2H_2 over a cordierite monolith previously coated with cobalt containing mordenite synthesized by a hydrothermal route, leading to the formation of ~20-μm thick layer of CNFs (hollow nanofibers 40–50 nm in diameter with closed ends) which increased the SSA of the component. Wang et al. [255, 256] circumvented the presence of the washcoat and synthesized CNTs directly on cordierite honeycombs (300 cpsi) via in situ CCVD of a C_2H_2/H_2 mixture over Fe or Co catalyst deposited by impregnation from a nitrate solution. The honeycombs possessed a SSA value of 30–40 m^2/g, suitable pore size distribution and good attachment of the CNTs layer (<1-μm thick) to the substrate. Jayaseelan et al. [257] produced SiC nanofibers on the surface of cordierite honeycombs via the carbothermal reduction reaction of carbon added to the oxide raw materials, when processing in inert atmosphere, leading to a SSA value of 36 m^2/g.

Ceramic foams have also been used as substrate for the growth of nanofibers and nanotubes. It has been shown that

a $Mg_{0.9}Co_{0.1}Al_2O_4$ solid solution foam prepared by gel-casting (total porosity 98%, cell window size < 300 μm), unlike the corresponding particulates, gave a 4-fold increase in the production of CNTs (>95% with only 1 or 2 walls, and ~70% single wall CNTs, SW-CNTs), because it allowed for a higher quantity of metal nanoparticles on the surface, a better dispersion of the metal particles (which hampers growth and therefore favors selectivity for CNTs formation), and increased space available for the growth of CNTs [258]. A commercial open cell ceramic foam (containing α-alumina (>80 wt%), mullite and cristobalite; 50 ppi, cell size 0.5–1.5 mm) was also impregnated by a slurry of α-$Al_{1.8}Fe_{0.2}O_3$ and covered by CNTs via CCVD [259]. In a similar way, a α-$(Al_{1-x}Fe_x)_2O_3$ foam was very recently also used to form CNTs [260]. As the above studies were more concerned with the production of CNTs per se, rather than in the development of components with high SSA, no information were given on the SSA and the mechanical properties of the final foams. Cordier et al. [261] using 50 ppi commercial alumina-silicate foams impregnated with a slurry of $Mg_{(1-x)}(Co_{0.75}Mo_{0.25})_xO$ ($X = 0.01$–0.2) followed the formation of CNTs via CCVD, clearly showed the formation of monoliths with a multi-scale pore structure including very well-distributed CNTs, giving a surface area of ~15 m^2 per gram of foam [261].

Pham-Huu and Ledoux [262] and recently Wenmakers et al. [263] deposited Ni on RVC (60 ppi, porosity 97 vol%) and produced CNFs by reaction with ethylene at 500 °C. Different types of CNF structures with a large nanofiber diameter distribution (30–1100 nm) were observed, and while no correlation could be made between nanofiber diameter and SSA of the monoliths, high values ranging from 118 to 146 m^2/g were produced. Mukhopadhyay et al. [264] also utilized commercial carbon foams (porosity 80 vol%) to grow CNTs via two-stage CVD, using a ferrocene catalyst, and showed that with a silica coating, not only higher iron deposition level could be obtained, but also the bond strength between CNTs and substrate was improved. By following a parallel strategy, Vanhaecke et al. [265] produced SiC nanofibers in the macropores of a SiC foam (45 ppi, cell size ~ 1.9 mm and SSA ~ 50 m^2/g) by converting the CNFs that formed on the SiC host structure via CCVD, using SiO vapor as a reactant at 1300 °C. The final SSA value for SiC–NFs/SiC foam was 50 m^2/g, lower than that of the foam covered with CNFs, because of the increase of the nanofibers diameter after reaction. The produced samples were tested in a diesel particulate filtration system, and the microstructure of the composite foam, comprising a macroscopic interconnected porosity and walls covered with nanofibers, led to a small pressure drop and high trapping efficiency during the filtration step of fine and ultrafine soot [265, 266].

The release of decomposition gases which occurs when pyrolyzing preceramic polymers at high temperature in inert atmosphere, has led to the development of 1D-nanostructures via CAP [257–270]. For instance, in situ formation of β-SiC nanowires was observed in the channels of porous SiC ceramics fabricated from β-SiC powder and PCS precursor used as a binder [271, 272]. Catalyst particles for the growth of the nanowires were considered to originate from unwanted iron impurity in the starting SiC powder [271, 272], but the amount of nanofibers formed was quite limited. Yoon et al. [273] reported the formation of highly aligned macroporous SiC ceramics decorated with homogenously distributed SiC nanowires, produced by unidirectional freeze casting of SiC/camphene slurries with different amounts of a preceramic polymer. Iron originated again from the starting SiC powder (i.e., no catalyst was added specifically for aiding the growth of nanostructures), and was found in the tips of the nanowires. The presence of 1D nanostructures led to a remarkable increase of SSA (from 30 to 86 m^2/g), when the initial preceramic polymer content was varied from 5 to 20 wt%, due to enhanced growth of the SiC nanowires.

A deliberate application of this processing concept, which uses the decomposition product of a preceramic polymer for the growth of nanofibers specifically on the surface of cellular polymer-derived-ceramic, is currently being pursued in our laboratory [269, 270, 274]. We focused on the deliberate one-pot synthesis of foams with hierarchical porosity via CAP using different catalysts (Fe, Co, Pt) and preceramic polymers (polysiloxanes and polysilazanes). In this way, cellular SiOC ceramics, possessing a large amount of interconnected porosity (>60 vol%) were produced by direct foaming, and the addition of a catalyst enabled the formation of 1D nanostructures (nanowires) in large quantity on the surface of the cell walls. The characteristics of the nanostructures depended on the preceramic polymer (Si/C/O ratio) and pyrolysis conditions (atmosphere and temperature). In particular, when heating in N_2, single crystal Si_3N_4 nanowires were obtained, while pyrolysis in Ar produced SiC nanowires. The formation of nanowires and their structural evolution (thickness, entanglement) caused a variation in the final SSA of the produced composite foams, which ranged from 10 to 110 m^2/g [269, 270]. In Fig. 6c and d, the morphology of components produced via CAP, showing Si_3N_4 nanowires coating the cell walls, is reported. The use of a Pt catalyst led to the formation of Pt-silicide tips which were active in the CO oxidation reaction; it is forecasted that the immobilization of the catalyst on the tip of nanofibers exposed to the environment could lead to increased efficiency and reduced catalyst loss during operation. Moreover, in a separate experiment, the presence of long nanofiber bundles decorating the cell walls

have been demonstrated to be very effective in the trapping of nanopowders (diameter ~ 90 nm) contained in a gas stream.

Etching

In the classical "Vycor" process, a homogeneous glass (usually in the Na_2O–B_2O_3–SiO_2 system) is prepared by the melt-quench method and heat treated to produce spinodal decomposition into two interconnected phases. After that, one phase is preferentially etched in a suitable acid, leaving behind a glass with 3D interconnected porosity. This method has recently been successfully used in making hierarchically porous bioglass samples which had multimodal meso–macro interconnected porosity (the average size of the macropores was about 32 μm with additional distinct pores within the 0.1–8-μm range and mesopores with average size 15 nm) [275, 276].

Very limited studies have used this concept to create multi-modal pore architecture, most probably due to the difficulty in controlling the phase separation and the harsh processing conditions required. Polymer-derived ceramics, in this respect, are very advantageous since phase separation is a common phenomenon for these materials [159, 277]. Wilson et al. [278] have shown that dilute HF etching of bulk SiOC glasses develops microporosity associated to a mass loss up to 40 wt%. This approach has been pursued further by the group of Soraru [279–281] for sol–gel-derived SiOC ceramics with different chemical compositions (varying Si/C/O ratio), and the results show that high SSA (600 m^2/g) can be obtained. While these samples did not include intentionally introduced macroporosity, Biasetto et al. [282] recently showed that microcellular SiOC samples (84 vol% porous with ~35 μm average cell size) can be etched by HF to produce high SSA (up to 65 m^2/g) foams with multi-modal porosity.

Selective phase/element etching has also been applied to other materials, e.g., cordierite, zeolite, or carbonbased cellular materials were acid-treated to increase their SSA, to create anchoring sites for the catalyst particles, or to reduce the thermal expansion coefficient [9, 188, 193, 244, 263, 264, 283]. Metal carbides have also been etched using halogen gases to manufacture ultra high SSA (~3000 m^2/g) carbon components (this microporous carbon is termed CDC) [285]. In this manner, very recently hierarchically porous (meso/micro) high SSA carbon samples have also been prepared from polymer-derived SiCN [286] and SiC [287, 288] ceramics. Alternatively, to form hierarchically porous carbon monoliths, a silica/carbon composite material can be formed by nanocasting of a carbon source into a porous silica monolith, followed by the leaching out the silica phase via chemical etching, to obtain a negative porous carbon replica [64, 65, 289, 290].

Use of preceramic polymers

One of the most effective methods for producing high SSA ceramics is to perform a well-controlled heat treatment cycle to preceramic polymers. This approach takes advantage of the transient porosity generated upon heat treating a precursor in the temperature range at which the polymer-to-ceramic conversion occurs [159]. The transformation generally occurs in the ~400–800 °C temperature range, and is accompanied by shrinkage and density increase [291, 292]. The build-up of internal pressure in the component, provoked by the decomposition of the organic moieties of the preceramic polymer (with generation of mainly CH_4 or C_6H_6), leads to the formation of porosity (with pore size typically below 50–100 nm). This porosity is transient, because it is eliminated when the pyrolysis temperature is increased, leading to the completion of the ceramization process according to a densification mechanism based on surface reaction/pyrolysis accommodated by viscous flow [292]. However, by employing a well-controlled heat treatment cycle and limiting the pyrolysis temperature to 500–700 °C, it is possible to stabilize and maintain this porosity, and therefore achieve components with very high SSA values (up to ~650 m^2/g) [293–297]. This approach has been successfully applied to foams produced from silicones [298], obtaining monoliths with hierarchical porosity in which the amount of SSA was stable up to the pyrolysis temperature reached, even after prolonged heating at the same temperature.

Properties and applications of ceramics with hierarchical porosity

The processing strategies discussed above lead to the fabrication of components possessing very varied morphologies and different properties (for instance, SSA values, permeability to fluids, mechanical strength, durability). It is however very difficult to discuss in detail the effect of the various fabrication methods on the properties of these components, as very limited and quite scattered information is available in the literature, making it hazardous to draw general conclusions. We can however highlight some of the properties and requirements which are of interest for the applications, especially those involving the presence of catalysts.

Heck et al. [299] reviewed the applications of cellular monoliths for the following applications: three way catalysts, diesel catalysts, ozone abatement in aircraft, natural gas engines, ozone destruction on automobile radiators, CO and hydrocarbon oxidation small engines, selective reduction of NO_x, catalytic combustion and the destruction of volatile organic compounds from chemical plants,

Table 1 Some examples of the application of macroporous cellular materials with multiscale pore hierarchy

	Material	Test type	Comments	Reference
Polymeric foam templating	Titanium silicalite-1	Catalytic activity for 1-hexene and 2,5-dihydrofuran epoxidation using H_2O_2 as an oxidant	Diffusion plays an important role in the catalysis of the liquid-phase epoxidation reactions	[71]
	ZSM-5 with various framework Si/Al ratios	Catalytic activity in methanol to olefin conversion	The ZMF catalyst with high macroporosity exhibited superior catalytic activity compared to its pelletized form, especially at higher feed flow rates, that signifies the importance of the macroporous structure in facilitating the enhanced mass transport for the labile diffusion of light olefins	[72]
Biological templates	TiO_2	Photocatalytic activity in CH_3CHO degradation	The samples are photocatalytically active, with kinetic constant values much larger than those of commercial TiO_2 catalysts (e.g. Degussa P25)	[98]
Phase separation	Silica	Pressure drop and column efficiency	The porous silica rods exhibit the weak dependence of HETP (height equivalent to a theoretical plate) on mobile phase velocity as well as the very low pressure drop, which enables performing high-speed analysis using conventional HPLC apparatus	[131]
	Silica	Separation efficient for polypeptides	More efficient separation than a conventional column packed with 5 μm wide pore silica particles	[132]
Rapid prototyping and templating	Bioactive glass	In vitro bone forming activity	Hydroxyapatite formed on the surface of the bioglass scaffold upon soaking in simulated body fluid for 24 h	[147]
	Zeolite/glass composite	Catalytic activity in *n*-hexane cracking	High activity in *n*-hexane cracking and higher selectivity towards C_2–C_3 light olefins, compared with commercial catalysts	[148]
Gel casting of ordered mesoporous silica precursors	Silica	HPLC columns	Good resolution with extremely low hydraulic resistance and rapid separation. Both the macropores and the mesopore modes can be adjusted, tailoring the hydraulic resistance of the column	[154]
Alumina coatings	Ni/Al_2O_3-washcoated cordierite honeycomb	Catalytic behavior in the autothermal reforming (ATR) of isooctane	Monoliths deactivate slowly with time on stream during ATR of isooctane. Loss of surface area by sintering also result in encapsulation of active components and loss of activity	[172]
	Pd/Al_2O_3-washcoated cordierite honeycomb	Hydrogenation of sunflower oil	At the same conversion and operating conditions, the structured catalysts presented a lower formation of trans-isomers than the Pd/Al_2O_3 powder. After three consecutive hydrogenation tests, no change in activity and selectivity was observed for the ceramic monolith	[175, 176]
	γ-Al_2O_3 washcoated α-Al_2O_3 foams	Pressure drop relationship	Results suggest that roughness introduced by the washcoat plays a dominant role in the turbulent resistance	[167]
		Mass and heat transport properties	Radial heat transfer coefficients for foams were two to five times higher than those predicted from correlations for packed beds	[168]
	Rh and Pt–Re bimetallic supported γ-Al_2O_3 washcoated α-Al_2O_3 foams	Dry reforming of methane with carbon dioxide.	Washcoating provided uniform deposits of Rh or Pt–Re complexes. While Rh is the best overall catalyst, Pt–Re is an attractive alternative for purely dry reforming	[175]

Table 1 continued

	Material	Test type	Comments	Reference
Zeolite coatings	ZSM-5 coated cordierite honeycomb	NH_3-TPD and propane gas adsorption	Compared to powder samples, ZSM-5 coated honeycomb samples have superior adsorption properties which are expected to be enhanced under flowing conditions because of the higher reactive surface area resulting from the loading of the ZSM-5 films on the honeycombs	[188, 193]
	ZSM-5 coated cordierite honeycomb	Selective reduction of NO_x with methane under oxygen excess	It is observed that the activity of the monolithic catalyst is as good as the one for zeolite powder, which indicates that there are no diffusive restrictions due to coating thickness	[187, 211]
	Cu-ZSM-5/cordierite honeycomb	Selective reduction of NO*x* by propane in excess oxygen and direct decomposition of NO	Cu-ZSM-5/cordierite was found to exhibit an enhanced turnover frequency compared to Cu-ZSM-5 powder, which make it a potential deNOx catalyst for future applications	[186]
	Cu-ZSM-5-coated cordierite honeycomb and alumina foam slabs	Selective reduction of NO_x by excess ammonia	~95% catalyst effectiveness was found for monoliths	[199]
	Zeolite (BEA, FAU)coated cordierite honeycomb	Activity in the acylation of aromatics	Coating a monolithic carrier with zeolites results in an active and selective integrated catalyst-reactor configuration for the acylation of aromatics	[209, 210]
	ZSM-5 coated mullite-bonded alumina foam	Conversion of methanol to olefins	The use of ZSM-5-coated ceramic foam packing in the conversion of methanol to olefins showed substantial activity and selectivity improvements as compared with conventional extruded zeolite pellets. The formation of propylene was particularly favored over the coated foams	[213]
	Zeolite coated β-SiC foam	Conversion of methanol to olefins	The use of ZSM-5 coated β-SiC foam packings in the methanol-to-olefins reaction present substantial activity/selectivity improvements compared to conventional zeolite packings. Moreover, the structured composites exhibit a higher stability toward deactivation by coking, compared to the powdered form of the zeolite	[214, 215]
Carbon coatings	Pd and Pt deposited on carbon coated cordierite honeycomb	Low-temperature catalytic combustion of xylenes	No gasification of the carbon-coated monoliths was observed during the catalytic combustion of xylene. Both Pd and Pt monolithic catalysts were active in this reaction	[235]
	Pd deposited on carbon coated cordierite honeycomb modified with α-Al_2O_3 (non-porous), micro and mesoporous composite carbon/ceramic monoliths	Low-temperature catalytic combustion of *m*-xylene	A strong interplay was found between the carbon porosity, macro- and mesopores, and its performance in the Pd catalyzed total combustion of *m*-xylene. Macro-Meso pores improve the contact between the Pd particles and the *m*-xylene molecules	[243]

Table 1 continued

	Material	Test type	Comments	Reference
	Pd deposited on carbon coated cordierite honeycomb modified with α-Al_2O_3, micro and mesoporous composite carbon/ceramic monoliths	Selective hydrogenation of fatty acid methyl esters of sunflower oil (FAME)	The Pd/carbon (nearly non-porous) coated cordierite honeycomb catalyst showed a superior selectivity performance compared to the micro-meso porosity including composite carbon/ceramic monoliths which suffered from pore diffusion limitations in the partial hydrogenation of FAME. This behavior is ascribed to the much shorter diffusion distances of the reactants and products, because of the Pd particles are placed at the external non-porous surface of the carbon layer.	[236, 237]
	Vanadium oxide deposited on carbon coated cordierite honeycomb	Selective reduction of NO_x by excess ammonia in the presence of oxygen	Carbon-supported vanadia is not deactivated by SO_2 at low temperatures. Moreover, high surface area of carbon and the possibility of maximizing the hydroxylation enabled it to disperse a higher amount of active phase per weight of support. It was found that mesoporosity of carbon support plays a key role on the resistance to SO_2 deactivation at low temperatures	[238–242]
	Vanadium oxide deposited on carbon coated cordierite honeycomb	Selective reduction of NO_x by excess ammonia	The experiments performed in a power plant reveal a substantial loss of catalytic activity even for short periods of residence in the exit stream of the power plant. Loss of catalytic activity seems to be caused predominantly by As poisoning and surface sulfates	[233, 234]
	Carbon coated cordierite honeycomb	Dynamic adsorption performance	High adsorption efficiency was obtained even with high flow rate and low concentration flow streams	[245]
	Carbon coated ceramic foams (zirconia stabilized with MgO) and alumina	Organic vapor adsorption	The coated foams displayed a reduced pressure drop compared to carbon granules and had good dynamic hexane vapor adsorption characteristics	[249]
1D-nanostructures	Carbon and CNF coated cordierite and acicular mullite honeycombs	Enzyme immobilization	With respect to catalysis, the open wall structure of ACM monoliths allows high and accessible catalyst loadings. More carbon was deposited per unit wall volume, thus more enzyme was immobilized, and more active honeycomb biocatalyst were prepared with the ACM monoliths compared to cordierite honeycombs	[246–248]
			Carbon fibers are the most promising enzyme supports in organic solvents	
	Ba-Ru/CNTs cordierite honeycombs	NH_3 synthesis	Barium promoted ruthenium catalysts supported on the as-synthesized materials showed much higher activity for ammonia synthesis than their counterparts deposited on pure cordierite monoliths	[255]
			The catalytic activity linearly increased with the BET surface area of CNTs-cordierite monoliths	
	Pd/Pt deposited on CNF and γ-Al_2O_3 coated cordierite honeycomb	Low-temperature catalytic combustion of benzene, toluene and *m*-xylene (BTX)	The catalysts supported on CNF-coated monoliths were more active than the γ-Al_2O_3-coated ones, independently on the metal catalyst or the type of the tested aromatic compound	[253]

Table 1 continued

	Material	Test type	Comments	Reference
	Ir/Pt/NiS_2 deposited on cellular 1D carbon materials	Several catalytic reactions: decomposition of hydrazine for satellite maneuvering, low-temperature selective oxidation of H_2S into elemental sulfur and a fuel cell (PEMFC)	The high external surface area and the absence of ink-bottled pores inside these materials significantly improve the reactants and products diffusion, which contribute to an increase of the catalytic activity and selectivity The existence of a strong interaction between the deposited active phase and the CNF surface could also led to a peculiar electronic alteration of the supported active phase and catalytic behavior	[262]
	SiC NFs-decorated SiC foam	Pressure drop experiments/Diesel particulate filtration	Macroscopic interconnected porosity and walls covered with nanofibers, led to a small pressure drop and high trapping efficiency during the filtration step of fine and ultrafine soot as in the case of a gasoline exhaust engine	[265, 266]
Preceramic polymer	Porous SiOC and Ni/Pt deposited on porous SiOC	Dynamic sorption behavior/CO oxidation	Amount of adsorbed hydrocarbons increased with total micro- and mesopore volume. The most important advantage of these materials is the possibility to completely eliminate the adsorbed species from the adsorber. Metallic Pt in the material is accessible to gases and shows good catalytic activity in CO oxidation	[296, 297]

domestic sources, and restaurants. Other emerging applications include: hydrogen generation for fuel cells, steam reforming of hydrocarbons, water gas shift catalysis, preferential oxidation of CO at low temperatures (CO-PROX), and also the production of chemicals such as H_2O_2, nitric acid, alkanes, or the transformation of paraffins into olefins. Some of the applications investigated so far using hierarchically cellular components with hierarchical porosity (mainly given by the presence of a washcoat or o coating based on zeolites or nanofibers) have been summarized in Table 1. As it can be deduced from the table, these materials have been mainly used either as adsorbents or in catalytic application with the help of deposited metallic sources. Besides for gas–solid catalytic processes, they can also be used successfully in the processing of high throughput gas streams (end-of-pipe exhaust control, burners).

Structured catalysts consist of catalytically active materials supported on cellular ceramic monoliths. Key benefits of these components over conventional-packed particles beds are the possibility to operate at high space velocity with low pressure drop and the capability of shaping the catalytically active material as a thin layer having low diffusional resistance, which is very advantageous for gas–solid catalytic processes with short contact times and high reaction rates. These features afford to the cellular components substantial improvements of selectivity in processes where the target product is the intermediate of a successive reaction pathway [212]. Additionally, these components possess high-geometric surface, high strength, high relative stiffness, low weight; furthermore, the use of preformed structures can simplify loading and unloading operations of the reactor [300]. In comparison to honeycomb monoliths, foams offer in addition to the low pressure drop the advantage of a turbulent flow enhancing the mass and heat transfer between the fluid phase and the catalyst washcoat, and they also allow radial mixing. The tortuous flow paths through the porous matrix enhance gas/solid heat- and mass transfer rates, and high surface-to-volume ratios yield high activity per unit reactor volume [212]. The use of metal, rather than ceramic, foams can minimize the occurrence of hot spots in the catalyst when highly exothermic reactions are performed, while avoiding mechanical-strength and thermal-shock limitations [301].

Processing strongly affects important properties such as relative density (i.e., total porosity), cell window size, strut thickness, and strut roughness [266, 302, 303], all features of significance for the tailoring of the permeability of the parts. Adjustment of axial or radial flow patterns in a reactor can be obtained by variations of the manufactured pore morphologies. The strength of monoliths with hierarchical porosity based on coatings on a macroporous

Table 2 From micro- and mesoporosity to multiscale pore hierarchy

Processing route	Composition	SSA (m^2/g)	Pore size (micro/meso)	Pore size (macro)	Reference
"Hard sphere" colloidal templating	SiO_2	173–1337	<2–9 nm	140–800 nm	[34, 45, 46, 49, 50, 52]
	TiO_2, $Al_2O_3{\cdot}xH_2O$, ZrO_2, Fe_2O_3, Sb_4O_6, WO_3, $Y_{0.043}Zr_{0.957}O_2$, Carbon	18–760	10.5–21.1 nm	400–700 nm	[34, 47]
	Al_2O_3	200–260	4–6 nm	50–320 nm	[36, 37]
"Hard sphere" colloidal templating, one-pot strategy	SiO_2	46–1000	<2 nm, 3–8 nm	80–800 nm	[35, 53–55, 62]
	Zeolite	650	<2 nm	100–300 μm	[56, 57]
Impregnation of "hard" transitional templates	Co_3O_4, SnO_2, MnO_2, Mn_2O_3	30–70	3–30 nm	0.5–30 μm	[63, 64]
	Carbon	1000–1500	2–8 nm	0.5–30 μm	[65, 66]
Impregnation of PU foam	Zeolitic foams	450–1000	2–3 nm	>100 μm to mm	[69–74]
	Silica, carbon	560–1860	3.4–8 nm	10–250 μm,	[75, 79]
	γ-Al_2O_3, NiO_2Al_4	178–241	2.9–3.4 nm	300–600 μm	[78]
Impregnation of UF foam	SiO_2, TiO_2, ZrO_2	4–324	3–4 nm	0.2–5 μm	[76, 77]
Biological templates	Zeolites	~10–500	<2 nm	0.5–50 μm	[85–97]
	SiO_2, TiO_2, SiC	14–650	2–50	50–200 μm	[98, 99, 101, 103–105]
Oil-in-formamide emulsion	TiO_2	20–700	1–10 nm	390 nm–~10 μm	[114–116]
Oil-in-water emulsion	SiO_2	250–1100	1–10 nm	0.3–3 μm	[119–121]
Mechanically induced emulsion	SiO_2	100–1000	1–40 nm	100–2000 μm	[117, 118, 122]
Phase separation	SiO_2, TiO_2	50–400	0.5–30 nm	0.5–10 μm	[126, 127, 129, 131, 132, 142]
Phase separation with surfactants	SiO_2	180–1000	3–20 nm	200 nm–20 μm	[134, 135, 138, 140]
Gel casting	SiO_2	516	0.5–16 nm	1–5 μm	[152, 154]
Pulsed current processing	SiO_2	2–275	7.5	0.1–0.4 μm	[155, 156]
One-pot direct foaming	SiOC	136	2.6 nm	100–500 μm	[157]

Type of material, SSA, pore size (micro/meso and macro) as a function of the processing route

ceramic body is generally higher than that of components in which macroporosity is introduced into micro–mesoporous materials, because of the lack of pores in the struts, which constitute the supporting structural elements [304]. Furthermore, the mass and heat (convective and radiative) transfer properties are also affected by the architecture of the part [305, 306]. In order to assess the influence of the morphology, which is directly related to the processing procedure adopted, on the main properties of a porous monolith it is necessary to perform a quantitative characterization of its geometry (characteristic path length, geometric surface area, and porosity) [307].

Concerning the durability and stability of porous structures, we can point out that it depends mainly on the specific environment of the considered application and on the composition of the material, as well as on the morphology of the monolith. Corrosion and erosion phenomena depend on the flow patterns as well as on the pore size and pore volume, and pore sintering depends on the pore characteristics and the operating temperature; therefore, variations in the fabrication process leading to changes in the pore architecture will affect the performance of the component.

In Tables 2 and 3, we summarize the main structural features of components possessing hierarchical porosity, as gathered from the aforementioned literature, as a function of the processing route.

Future perspectives

As highlighted above, numerous strategies exist for the fabrication of ceramic monoliths possessing hierarchical porosity. However, some of the proposed techniques are somewhat cumbersome and thus best suited for small scale, laboratory operations. Further progress in fabrication methods is therefore needed to increase the size of the components, reduce their cost, and address the specific

Table 3 From macroporosity to multiscale pore hierarchy

Processing route	Layer	SSA (m^2/g)	Pore size (micro/meso)	Pore size (macro)	Reference
Coating strategies	γ-Al_2O_3	20–50	5–20 nm	Honeycombs 200–600 cpsi	[2, 166–169, 174, 251]
	Zeolites	6–212	<2 nm	Honeycombs 200–600 cpsi and macrocellular foams 1500–3000 μm	[186, 192–194, 196–199, 209, 210]
	Zeolites	19–453	0.5–20 nm	Macrocellular foams 100–1000 μm	[102, 148, 214, 215, 221]
	Zeolites	113–541	10–30 nm	Microcellular foams ~1–8 μm	[220, 222–224]
	Mesoporous silica (MCM-41)	7–229	2–5 nm, 20–70 nm	Macrocellular foams ~100–1500 μm	[225–227]
	Carbon	390–680	<1 nm	Honeycombs 200–600 cpsi	[232, 233, 244, 248]
	Carbon	236–697	3.7–50 nm	Macrocellular foams 2500–4500 μm	[249, 250]
Growth of 1D nanostructures	CNFs	25–70.0	8–17 nm	Honeycombs 400–600 cpsi	[173, 174, 246–248, 251–253]
	CNFs	60–146	N/A	Macrocellular foams 1200–1500 μm	[262, 263, 265]
	CNTs	15–42	1–10 nm	Honeycombs 300 cpsi	[255, 256]
	CNTs	15	N/A	Macrocellular foam 1500 μm	[261]
	SiC	24–36	N/A	Honeycomb 600 cpsi	[257]
	SiC	19–50	N/A	Macrocellular foam 1800 μm	[265]
	SiC	30–86	N/A	Microcellular foam 12–14 μm	[273]
	SiC	15–84	0.7 nm, 3.7–22.6 nm	Macrocellular foam 100–500 μm	[269, 270]
	Si_3N_4	10–110	0.7 nm, 3.7–15 nm	Macrocellular foam 100–500 μm	[269, 270]
Etching		N/A	15 nm	Microcellular foam 0.1–32 μm	[275, 276]
		65	3–5 nm	Microcellular foam 35 μm	[282]
		0.9–255	1.5-3.5 nm	Honeycombs 300–500 cpsi	[284]
Use of preceramic polymers		654	<2 nm	N/A	[296]
		13–436	3–4.5 nm	Macrocellular foam 80–800 μm	[298]

Type of material, SSA, pore size (micro/meso and macro) as a function of the processing route

requirements of some applications. For instance, an increase in the total amount of porosity, but maintaining the same level of strength, is desired for specialized applications such as Diesel particulate filters, where a decrease in the pressure drop and an increase of trapping efficiency would be highly beneficial. For other applications, such as protein sorption, it would be valuable to widen even further the range of (meso-)pore sizes achievable, and develop a tighter control on the pore morphology.

Components with such a complex architecture require the simultaneous use of several analytical techniques for analyzing their porosity at all length scales. Advances in 3D imaging techniques, such as computer-assisted tomography, would enable routine quantification of the pore morphology, providing also useful data for much-needed modeling of the component properties.

Finally, further developments in the functionalization of ceramics with hierarchical porosity, for instance by adding catalytic capabilities, electrical conductivity, piezoelectricity, or ferromagnetic properties to the same component, will lead to more versatile filters and to devices possessing an even wider set of properties, for use in advanced applications in several fields, including medicine, environmental, and chemical engineering.

References

1. Colombo P (2008) Science 322:381
2. Twigg MV, Richardson JT (2007) Ind Eng Chem Res 46:4166
3. Schüth F, Sing KSW, Weitkamp J (2002) Handbook of porous solids. Wiley-VCH Verlag GmbH, Weinheim
4. Freyman TM, Yannas IV, Gibson LJ (2001) Prog Mater Sci 46:273
5. Haber J (1991) Pure Appl Chem 63:1227
6. Martini-vvedensky JE, Suh NP, Waldman FA (1984) US Patent 4473665

7. Colombo P, Bernardo E, Biasetto L (2004) J Am Ceram Soc 87:152
8. Roquerol J, Avnir D, Fairbridge CW et al (1994) Pure Appl Chem 66:1739
9. Avila P, Montes M, Miró EE (2005) Chem Eng J 109:11
10. Yuan Z-Y, Ren T-Z, Su B-L (2004) Chem Phys Lett 383:348
11. Kooyman PJ (2008) Stud Surf Sci Catal 174:91
12. Huiyong C, Hongxia X, Xianying C, Yu Q (2009) Microporous Mesoporous Mater 118:396
13. Li K (2007) Ceramic membranes for separation and reaction. Wiley, Chichester
14. Schüth F (2003) Angew Chem Int Ed 42:3604
15. Colombo P (2006) Philos Trans Roy Soc A 364:109
16. Studart AR, Gonzenbach UT, Tervoort E, Gauckler LJ (2006) J Am Ceram Soc 89:1771
17. Soler-Illia G, Sanchez C, Lebeau B, Patarin J (2002) Chem Rev 102:4093
18. Tiemann M (2008) Chem Mater 20:961
19. Malfatti L, Kidchob T, Costacurta S et al (2006) Chem Mater 18:4553
20. Cagnol F, Grosso D, Soler-Illia G et al (2003) J Mater Chem 13:61
21. Brinker CJ, Lu Y, Sellinger A, Fan H (1999) Adv Mater 11:579
22. Huo Q, Margolese DI, Ciesla U et al (1994) Chem Mater 6: 1176
23. Firouzi A, Atef F, Oertli AG, Stucky GD, Chmelka BF (1997) J Am Chem Soc 119:3596
24. Lu AH, Schüth F (2006) Adv Mater 18:1793
25. Dyer A (1988) An introduction to zeolite molecular sieves. Wiley, Chichester
26. Schmidt-Winkel P, Lukens WW, Yang P et al (2000) Chem Mater 12:686
27. Beck JS, Vartuli JC, Roth WJ et al (1992) J Am Chem Soc 114:10834
28. Kresge CT, Leonowicz ME, Roth WJ, Vartuli JC, Beck JS (1992) Nature 359:710
29. Yuan Z-Y, Su B-L (2006) J Mater Chem 16:663
30. Vantomme A, Léonard A, Yuan Z-Y, Su B-L (2007) Colloids Surf Physicochem Eng Aspects 300:70
31. Bergna HE, Roberts WO (eds) (2006) Colloidal silica, Fundamentals and applications. CRC Press, Boca Raton
32. Yang P, Deng T, Zhao D et al (1998) Science 282:2244
33. Holland BT, Blanford CF, Stein A (1998) Science 281:538
34. Holland BT, Blanford CF, Do T, Stein A (1999) Chem Mater 11:795
35. Sen T, Tiddy GJT, Casci JL, Anderson MW (2004) Chem Mater 16:2044
36. Dacquin J-P, Dhainaut J, Duprez D, Royer S, Lee AF, Wilson K (2009) J Am Chem Soc 131:12896
37. Kim Y, Kim C, Yi J (2004) Mater Res Bull 39:2103
38. Gundiah G (2001) Bull Mater Sci 24:211
39. Lekkerkerker HNW, Stroobants A (1998) Nature 393:305
40. Frenkel D (2006) Nature Mater 5:85
41. Stein A (2001) Microporous Mesoporous Mater 44–45:227
42. Wijnhoven JEGJ, Vos WL (1998) Science 281:802–804
43. Zakhidov AA, Baughman RH, Iqbal Z et al (1998) Science 282:897
44. Holland BT, Abrams L, Stein A (1999) J Am Chem Soc 121:4308
45. Sen T, Tiddy GJT, Casci JL, Anderson MW (2003) Angew Chem Int Ed 42:4649
46. Lebeau B, Fowler CE, Mann S, Farcet C, Charleux B, Sanchez C (2000) J Mater Chem 10:2105
47. Deng Y, Liu C, Yu T et al (2007) Chem Mater 19:3271
48. Vaudreuil S, Bousmina M, Kaliaguine S, Bonneviot L (2001) Adv Mater 13:1310
49. Oh CG, Baek Y, Ihm SK (2005) Adv Mater 17:270
50. Danumah C, Vaudreuil S, Bonneviot L, Bousmina M, Giasson S, Kaliaguine S (2001) Microporous Mesoporous Mater 44–45:241
51. Valtchev V, Mintova S (2001) Microporous Mesoporous Mater 43:41
52. Rhodes KH, Davis SA, Caruso F, Zhang B, Mann S (2000) Chem Mater 12:2832
53. Antonietti M, Berton B, Göltner C, Hentze H-P (1998) Adv Mater 10:154
54. Suzuki N, Sakka Y, Yamauchi Y (2009) Sci Technol Adv Mater 10:025002
55. Luo Q, Li L, Yang B, Zhao D (2000) Chem Lett 29:378
56. Walsh D, Kulak A, Aoki K, Ikoma T, Tanaka J, Mann S (2004) Angew Chem Int Ed 43:6691
57. Madhusoodana CD, Das RN, Kameshima Y, Okada K (2005) J Porous Mater 12:273
58. Kuang D, Brezesinski T, Smarsly B (2004) J Am Chem Soc 126:10534
59. Seddon KR, Stark A, Torres M-J (2000) Pure Appl Chem 72:2275
60. Brezesinski T, Erpen C, Iimura K-i, Smarsly B (2005) Chem Mater 17:1683
61. Antonietti M, Kuang D, Smarsly B, Zhou Y (2004) Angew Chem Int Ed 43:4988
62. Zhou Y, Antonietti M (2003) Chem Commun 2564–2565
63. Smått J-H, Spliethoff B, Rosenholm JB, Lindén M (2004) Chem Commun 2188–2189
64. Smått J-H, Weidenthaler C, Rosenholm JB, Lindén M (2006) Chem Mater 18:1443
65. Taguchi A, Smått JH, Lindén M (2003) Adv Mater 15:1209
66. Lu AH, Smått JH, Lindén M (2005) Adv Funct Mater 15:865
67. Lu A-H, Smått J-H, Backlund S, Lindén M (2004) Microporous Mesoporous Mater 72:59
68. Davis SA, Breulmann M, Rhodes KH, Zhang B, Mann S (2001) Chem Mater 13:3218
69. Lee YJ, Lee JS, Park YS, Yoon KB (2001) Adv Mater 13: 1259
70. Lee Y-J, Yoon KB (2006) Microporous Mesoporous Mater 88:176
71. Kim WJ, Kim TJ, Ahn WS, Lee YJ, Yoon KB (2003) Catal Lett 91:123
72. Lee Y-J, Kim Y-W, Jun K-W, Viswanadham N, Bae J, Park H-S (2009) Catal Lett 129:408
73. Huerta L, Guillem C, Latorre J, Beltrán A, Beltrán D, Amorós P (2003) Chem Commun 1448–1449
74. Huerta L, Guillem C, Latorre J, Beltrán A, Beltrán D, Amorós P (2005) Solid State Sci 7:405
75. Álvarez S, Fuertes AB (2007) Mater Lett 61:2378
76. Shi Z-G, Xu L-Y, Feng Y-Q (2006) J Non-Cryst Solids 352:4003
77. Xu L-Y, Shi Z-G, Feng Y-Q (2007) Microporous Mesoporous Mater 98:303
78. Li L-L, Duan W-T, Yuan Q, Li Z-X, Duan H-H, Yan C-H (2009) Chem Commun 6174–6176
79. Giunta PR, Washington RP, Campbell TD, Steinbock O, Stiegman AE (2004) Angew Chem Int Ed 43:1505
80. Hall SR (2009) Biotemplating: complex structures from natural materials. World Scientific Publishing, Singapore
81. Mann S (2001) Biomineralization. Principles and concepts in bioinorganic materials chemistry. Oxford University Press, Oxford
82. Dujardin E, Mann S (2002) Adv Mater 14:775
83. Greil P (2001) J Eur Ceram Soc 21:105
84. Sieber H (2005) Mater Sci Eng B 412:43
85. Zhang B, Davis SA, Mann S (2002) Chem Mater 14:1369

86. Li J, Xu Q, Wang J, Jiao J, Zhang Z (2008) Ind Eng Chem Res 47:7680
87. Dong A, Wang Y, Tang Y et al (2002) Adv Mater 14:926
88. Valtchev V, Smaihi M, Faust A-C, Vidal L (2003) Angew Chem Int Ed 42:2782
89. Valtchev VP, Smaihi M, Faust A-C, Vidal L (2004) Chem Mater 16:1350
90. Xu J, Yao J, Zeng C, Zhang L, Xu N (2010) J Porous Mater 17:329
91. Liu W, Zhang L, Wang H, Xu N (2007) Stud Surf Sci Catal 170:408
92. Li G, Singh R, Li D, Zhao C, Liu L, Webley PA (2009) J Mater Chem 19:8372
93. Anderson MW, Holmes SM, Noreen H, Cundy CS (2000) Angew Chem Int Ed 39:2707
94. Wang Y, Tang Y, Dong A, Wang X, Ren N, Gao Z (2002) J Mater Chem 12:1812
95. Losic D, Mitchell JG, Voelcker N,H (2009) Adv Mater 21:2947
96. Davis SA, Burkett SL, Mendelson NH, Mann S (1997) Nature 385:420
97. Zhang B, Davis SA, Mann S, Mendelson NH (2000) Chem Commun 781–782
98. Iwasaki M, Davis SA, Mann S (2004) J Sol-Gel Sci Technol 32:99
99. Liu Z, Fan T, Zhang W, Zhang D (2005) Microporous Mesoporous Mater 85:82
100. Sieber H, Hoffmann C, Kaindl A, Greil P (2000) Adv Eng Mater 2:105
101. Vyshnyakova KL, Yushin G, Pereselentseva LN, Gogotsi Y (2006) Int J Appl Ceram Technol 3:485
102. Zampieri A, Kullmann S, Selvam T et al (2006) Microporous Mesoporous Mater 90:162
103. Shin Y, Wang C, Exarhos GJ (2005) Adv Mater 17:73
104. Shin Y, Liu J, Chang JH, Nie Z, Exarhos GJ (2001) Adv Mater 13:728
105. Wang L-Q, Shin Y, Samuels WD et al (2003) J Phys Chem B 107:13793
106. Forsyth PA, Marcelia S, Mitchell DJ, Ninham BW (1978) Adv Colloid Interface Sci 9:37
107. Bechinger C (2002) Curr Opin Colloid Interface Sci 7:204
108. Imhof A, Pine DJ (1998) Adv Mater 10:697
109. Soler-Illia G, Crepaldi EL, Grosso D, Sanchez C (2003) Curr Opin Colloid Interface Sci 8:109
110. Velikonja J, Kosaric N (1993) In: Kosaric N (ed) Biosurfactants: production, properties, applications (surfactant sciences series). Marcel Dekker, New York
111. Kabalnov A, Lindman B, Olsson U, Piculell L, Thuresson K, Wennerström H (1996) Colloid Polym Sci 274:297
112. Bibette J (1991) J Colloid Interface Sci 147:474
113. Imhof A, Pine DJ (1997) Nature 389:948
114. Imhof A, Pine DJ (1999) Adv Mater 11:311
115. Yi G-R, Yang S-M (1999) Chem Mater 11:2322
116. Yuan ZY, Ren TZ, Su BL (2003) Adv Mater 15:1462
117. Bagshaw SA (1999) Chem Commun 767–768
118. Carn F, Colin A, Achard MF, Deleuze H, Saadi Z, Backov R (2004) Adv Mater 16:140
119. Maekawa H, Esquena J, Bishop S, Solans C, Chmelka BF (2003) Adv Mater 15:591
120. Sen T, Tiddy GJT, Casci JL, Anderson MW (2003) Chem Commun 2182–2183
121. Sen T, Tiddy GJT, Casci JL, Anderson MW (2005) Microporous Mesoporous Mater 78:255
122. Carn F, Saadaoui H, Massé P et al (2006) Langmuir 22:5469
123. Stöber W, Fink A, Bohn E (1968) J Colloid Interface Sci 26:62
124. Blin J-L, Léonard A, Yuan Z-Y et al (2003) Angew Chem Int Ed 42:2872
125. Nakanishi K (1997) J Porous Mater 4:67
126. Nakanishi K (2000) J Sol-Gel Sci Technol 19:65
127. Konishi J, Fujita K, Nakanishi K, Hirao K (2006) Chem Mater 18:6069
128. Konishi J, Fujita K, Nakanishi K et al (2009) J Chromatogr A 1216:7375
129. Konishi J, Fujita K, Oiwa S, Nakanishi K, Hirao K (2008) Chem Mater 20:2165
130. Tanaka N, Kobayashi H, Nakanishi K, Minakuchi H, Ishizuka N (2001) Anal Chem 73:420A
131. Ishizuka N, Minakuchi H, Nakanishi K, Soga N, Tanaka N (1998) J Chromatogr A 797:133
132. Minakuchi H, Nakanishi K, Soga N, Ishizuka N, Tanaka N (1996) Anal Chem 68:3498
133. Nakanishi K, Minakuchi H, Soga N, Tanaka N (1998) J Sol-Gel Sci Technol 13:163
134. Smått J-H, Schunk S, Lindén M (2003) Chem Mater 15:2354
135. Hüsing N, Raab C, Torma V, Roig A, Peterlik H (2003) Chem Mater 15:2690
136. Göltner CG, Antonietti M (1997) Adv Mater 9:431
137. Nakanishi K, Kobayashi Y, Amatani T, Hirao K, Kodaira T (2004) Chem Mater 16:3652
138. Amatani T, Nakanishi K, Hirao K, Kodaira T (2005) Chem Mater 17:2114
139. Brandhuber D, Torma V, Raab C, Peterlik H, Kulak A, Husing N (2005) Chem Mater 17:4262
140. Shi Z-G, Feng Y-Q, Xu L, Da S-L, Ren Y-Y (2004) Microporous Mesoporous Mater 68:55
141. Zhong H, Zhu G, Wang P, Liu J, Yang J, Yang Q (2008) J Chromatogr A 1190:232
142. Backlund S, Smått JH, Rosenholm JB, Lindén M (2007) J Dispers Sci Technol 28:115
143. Deville S (2008) Adv Eng Mater 10:155
144. Nishihara H, Mukai SR, Yamashita D, Tamon H (2005) Chem Mater 17:683
145. Nishihara H, Iwamura S, Kyotani T (2009) J Mater Chem 18:3662
146. Nishihara H, Mukai SR, Fujii Y, Tago T, Masuda T, Tamon H (2006) J Mater Chem 16:3231
147. Yun H-S, Kim S-E, Hyeon Y-T (2007) Chem Commun 2139–2141
148. Ocampo F, Yun HS, Pereira MM, Tessonnier JP, Louis B (2009) Cryst Growth Des 9:3721
149. Nawrocki J, Dunlap C, McCormick A, Carr PW (2004) J Chromatogr A 1028:1
150. El Kadib A, Chimenton R, Sachse A, Fajula F, Galarneau A, Coq B (2009) Angew Chem Int Ed 48:4969
151. El Haskouri J, De Zárate DO, Guillem C, et al. (2002) Chem Commun 330–331
152. Wang H, Huang L, Wang Z, Mitra A, Yan Y (2001) Chem Commun 1364–1365
153. Dong D, Huang Y, Zhang X, He L, Li C-Z, Wang H (2009) J Mater Chem 19:7070
154. Liang C, Dai S, Guiochon G (2002) Chem Commun 2680–2681
155. Vasiliev PO, Shen Z, Hodgkins RP, Bergstrom L (2006) Chem Mater 18:4933
156. Akhtar F, Vasiliev PO, Bergström L (2009) J Am Ceram Soc 92:338
157. Vakifahmetoglu C, Pauletti A, Fernandez Martin C, Babonneau F, Colombo P (2009) Int J Appl Ceram Technol. doi: 10.1111/j.1744-7402.2009.02365.x
158. Gibson LJ, Ashby MF (1999) Cellular solids, structure and properties. Cambridge University Press, Cambridge
159. Colombo P (2008) J Eur Ceram Soc 28:1389
160. Scheffler M, Colombo P (eds) (2005) Cellular ceramics: structure, manufacturing, properties and applications. Wiley-VCH Verlag GmbH, Weinheim

161. Green DJ, Colombo P (2003) Mater Res Soc Bull 28:296
162. Meille V (2006) Appl Catal B 315:1
163. Nijhuis TA, Beers AEW, Vergunst T, Hoek I, Kapteijn F, Moulijn JA (2001) Catal Rev Sci Eng 43:345
164. Mitra B, Kunzru D (2008) J Am Ceram Soc 91:64
165. Buciuman F-C, Kraushaar-Czarnetzki B (2001) Catal Today 69:337
166. Jiang P, Lu G, Guo Y, Guo Y, Zhang S, Wang X (2005) Surf Coat Technol 190:314
167. Richardson JT, Peng Y, Remue D (2000) Appl Catal A 204:19
168. Richardson JT, Remue D, Hung JK (2003) Appl Cat A 250:319
169. Agrafiotis C, Tsetsekou A (2002) J Eur Ceram Soc 22:423
170. Narula CK, Allison JE, Bauer DR, Gandhi HS (1996) Chem Mater 8:984
171. Agrafiotis C, Tsetsekou A (2000) J Mater Sci 35:951. doi: 10.1023/A:1004762827623
172. Villegas L, Masset F, Guilhaume N (2007) Appl Catal B 320:43
173. Jarrah NA, Van Ommen JG, Lefferts L (2004) J Mater Chem 14:1590
174. Jarrah N, Van Ommen JG, Lefferts L (2003) Catal Today 79–80:29
175. Richardson JT, Garrait M, Hung JK (2003) Appl Catal B 255:69
176. Sánchez JF, González Bello OJ, Montes M, Tonetto GM, Damiani DE (2009) Catal Commun 10:1446
177. Deng S, Lin Y (1997) J Mater Sci Lett 16:1291
178. Agrafiotis C, Tsetsekou A, Ekonomakou A (1999) J Mater Sci Lett 18:1421
179. Agrafiotis C, Tsetsekou A (2000) J Eur Ceram Soc 20:815
180. Agrafiotis C, Tsetsekou A (2000) J Eur Ceram Soc 20:825
181. Corma A (1997) Chem Rev 97:2373
182. Davis ME (1998) Microporous Mesoporous Mater 21:173
183. Bein T (1996) Chem Mater 8:1636
184. Tavolaro A, Drioli E (1999) Adv Mater 11:975
185. Mizukami F (1999) Stud Surf Sci Catal 125:1
186. Li L, Xue B, Chen J et al (2005) Appl Catal B 292:312
187. Zamaro JM, Ulla MA, Miró EE (2005) Chem Eng J 106:25
188. Madhusoodana CD, Das RN, Kameshima Y, Yasumori A, Okada K (2001) J Porous Mater 8:265
189. Ulla MA, Miro E, Mallada R, Coronas J, Santamaria J (2004) Chem Commun 528–529
190. Jansen JC, Koegler JH, van Bekkum H et al (1998) Microporous Mesoporous Mater 21:213
191. Silva ER, Silva JM, Vaz MF, Oliveira FAC, Ribeiro F (2009) Mater Lett 63:572
192. Öhrman O, Hedlund J, Sterte J (2004) Appl Catal B 270:193
193. Okada K, Kameshima Y, Madhusoodana CD, Das RN (2004) Sci Technol Adv Mater 5:479
194. Ulla MA, Mallada R, Coronas J, Gutierrez L, Miró E, Santamaría J (2003) Appl Catal B 253:257
195. Basaldella EI, Kikot A, Bengoa JF, Tara JC (2002) Mater Lett 52:350
196. Aiello R, Crea F, Testa F, Spanti Gattuso A (1999) Stud Surf Sci Catal 125:29
197. Lin X, Kikuchi E, Matsukata M (2001) Stud Surf Sci Catal 135:162
198. Seijger GBF, Oudshoorn OL, Van Kooten WEJ et al (2000) Microporous Mesoporous Mater 39:195
199. Seijger GBF, Oudshoorn OL, Boekhorst A, Van Bekkum H, Van den Bleek CM, Calis HPA (2001) Chem Eng Sci 56:849
200. Sterte J, Hedlund J, Creaser D et al (2001) Catal Today 69:323
201. Falamaki C, Afarani MS, Aghaie A (2006) J Am Ceram Soc 89:408
202. Yan Y, Davis ME, Gavalas GR (1995) Ind Eng Chem Res 34:1652
203. Yan Y, Tsapatsis M, Gavalas GR, Davis ME (1995) J Chem Soc Chem Commun 227–228
204. Calis HP, Gerritsen AW, Bleek CMVD, Legein CH, Jansen JC, Bekkum HV (1995) Can J Chem Eng 73:120
205. Geus ER, den Exter MJ, van Bekkum H (1992) J Chem Soc Faraday Trans 88:3101
206. Yan Y, Davis ME, Gavalas GR (1997) J Membr Sci 123:95
207. Zhang L, Wang H (2003) J Mater Sci 38:1439. doi: 10.1023/A:1022904127678
208. Katsuki H, Furuta S, Komarneni S (2000) J Am Ceram Soc 83:1093
209. Beers AEW, Nijhuis TA, Kapteijn F, Moulijn JA (2001) Microporous Mesoporous Mater 48:279
210. Beers AEW, Nijhuis TA, Aalders N, Kapteijn F, Moulijn JA (2003) Appl Catal B 243:237
211. Zamaro JM, Ulla MA, Miró EE (2005) Catal Today 107–108:86
212. Patcas FC, Garrido GI, Kraushaar-Czarnetzki B (2007) Chem Eng Sci 62:3984
213. Patcas FC (2005) J Catal 231:194
214. Ivanova S, Louis B, Madani B, Tessonnier JP, Ledoux MJ, Pham-Huu C (2007) J Phys Chem C 111:4368
215. Ivanova S, Louis B, Ledoux M-J, Pham-Huu C (2007) J Am Chem Soc 129:3383
216. Louis B, Tezel C, Kiwi-Minsker L, Renken A (2001) Catal Today 69:365
217. Schwieger W, Rauscher M, Mönnig R et al (2000) Stud Surf Sci Catal 129:121
218. Scheffler F, Zampieri A, Schwieger W, Zeschky J, Scheffler M, Greil P (2005) Adv Appl Ceram 104:43
219. Scheffler M, Gambaryan-Roisman T, Zeschky J, Scheffler F, Greil P (2002) Ceram Eng Sci Proc 23:203
220. Zampieri A, Colombo P, Mabande GTP, Selvam T, Schwieger W, Scheffler F (2004) Adv Mater 16:819
221. Wang Y-Y, Jin G-Q, Guo X-Y (2009) Microporous Mesoporous Mater 118:302
222. Tong Y, Zhao T, Li F, Wang Y (2006) Chem Mater 18:4218
223. Lei Q, Zhao T, Li F, Wang Y, Zheng M (2006) Chem Lett 35:490
224. Lei Q, Zhao T, Li F, Wang Y, Hou L (2008) J Porous Mater 15:643
225. Huerta L, El Haskouri J, Vie D et al (2007) Chem Mater 19:1082
226. Costacurta S, Biasetto L, Pippel E, Woltersdorf J, Colombo P (2007) J Am Ceram Soc 90:2172
227. Granato T, Le Piane F, Testa F, Katovic A, Aiello R (2010) Mater Lett 64:1622
228. Vergunst T, Linders MJG, Kapteijn F, Moulijn JA (2001) Catal Rev Sci Eng 43:291
229. Gatica JM, Rodríguez-Izquierdo JM, Sánchez D, Ania C, Parra JB, Vidal H (2004) Carbon 42:3251
230. Moreno-Castilla C, Pérez-Cadenas AF (2010) Materials 3:1203
231. Alcañiz-Monge JA, Cazorla-Amorós D, Linares-Solano A, Morallón E, Vázquez J (1998) Carbon 36:1003
232. Vergunst T, Kapteijn F, Moulijn JA (2002) Carbon 40:1891
233. Valdés-Solís T, Marbán G, Fuertes AB (2001) Microporous Mesoporous Mater 43:113
234. Valdés-Solís T, Marbán G, Fuertes AB (2003) Appl Catal B 46:261
235. Pérez-Cadenas AF, Kapteijn F, Moulijn JA, Maldonado-Hódar FJ, Carrasco-Marín F, Moreno-Castilla C (2006) Carbon 44:2463
236. Pérez-Cadenas AF, Zieverink MMP, Kapteijn F, Moulijn JA (2006) Carbon 44:173
237. Pérez-Cadenas AF, Zieverink MMP, Kapteijn F, Moulijn JA (2007) Catal Today 128:13
238. Garcia-Bordeje E, Lazaro MJ, Moliner R, Galindo JF, Sotres J, Baro AM (2004) J Catal 223:395
239. Garcia-Bordeje E, Kapteijn EF, Moulijn JA (2001) Catal Today 69:357

240. Garcia-Bordeje E, Lazaro MJ, Moliner R, Álvarez PM, Gómez-Serrano V, Fierro JLG (2006) Carbon 44:407
241. Garcia-Bordeje E, Calvillo L, Lazaro MJ, Moliner R (2004) Ind Eng Chem Res 43:4073
242. García-Bordejé E, Monzón A, Lázaro MJ, Moliner R (2005) Catal Today 102–103:177
243. Pérez-Cadenas AF, Morales-Torres S, Kapteijn F et al (2008) Appl Catal B 77:272
244. Garcia-Bordeje E, Kapteijn F, Moulijn JA (2002) Carbon 40:1079
245. Gadkaree KP (1998) Carbon 36:981
246. De Lathouder KM, Marques Fló T, Kapteijn F, Moulijn JA (2005) Catal Today 105:443
247. De Lathouder KM, Lozano-Castelló D, Linares-Solano A, Kapteijn F, Moulijn JA (2006) Carbon 44:3053
248. De Lathouder KM, Bakker J, Kreutzer MT, Kapteijn F, Moulijn JA, Wallin SA (2004) Chem Eng Sci 59:5027
249. Dawson EA, Barnes PA, Chinn MJ (2006) Carbon 44:1189
250. Maldonado-Hodar FJ, Morales-Torres S, Ribeiro F et al (2008) Langmuir 24:3267
251. Garcia-Bordeje E, Kvande I, Chen D, Ronning M (2006) Adv Mater 18:1589
252. Garcia-Bordeje E, Kvande I, Chen D, Ronning M (2007) Carbon 45:1828
253. Morales-Torres S, Pérez-Cadenas AF, Kapteijn F, Carrasco-Marín F, Maldonado-Hódar FJ, Moulijn JA (2009) Appl Catal B 89:411
254. Ulla MA, Valera A, Ubieto T et al (2008) Catal Today 133–135:7
255. Gong B, Wang R, Lin B, Xie F, Yu X, Wei K (2008) Catal Lett 122:287
256. Wang J, Wang R, Yu X, Lin J, Xie F, Wei K (2006) J Nat Gas Chem 15:211
257. Jayaseelan DD, Lee WE, Amutharani D, Zhang S, Yoshida K, Kita H (2007) J Am Ceram Soc 90:1603
258. Rul S, Laurent C, Peigney A, Rousset A (2003) J Eur Ceram Soc 23:1233
259. Cordier A, Rossignol F, Laurent C, Chartier T, Peigney A (2007) Appl Catal B 319:7
260. De Resende VG, De Grave E, Cordier A, Weibel A, Peigney A, Laurent C (2009) Carbon 47:482
261. Cordier A, Flahaut E, Viazzi C, Laurent C, Peigney A (2005) J Mater Chem 15:4041
262. Pham-Huu C, Ledoux M-J (2006) Top Catal 40:49
263. Wenmakers PWAM, Jvd Schaaf, Kuster BFM, Schouten JC (2008) J Mater Chem 18:2426
264. Mukhopadhyay SM, Karumuri A, Barney IT (2009) J Phys D Appl Phys 42:195503
265. Vanhaecke E, Ivanova S, Deneuve A et al (2008) J Mater Chem 18:4654
266. Edouard D, Ivanova S, Lacroix M, Vanhaecke E, Pham C, Pham-Huu C (2009) Catal Today 141:403
267. Berger A, Pippel E, Woltersdorf J, Scheffler M, Cromme P, Greil P (2005) Phys Status Solidi A 202:2277
268. Scheffler M, Greil P, Berger A, Pippel E, Woltersdorf J (2004) Mater Chem Phys 84:131
269. Vakifahmetoglu C, Pippel E, Woltersdorf J, Colombo P (2010) J Am Ceram Soc 93(4):959
270. Vakifahmetoglu C, Carturan S, Pippel E, Woltersdorf J, Colombo P (2010) J Am Ceram Soc (in press)
271. Zhu S, Xi H-A, Li Q, Wang R (2005) J Am Ceram Soc 88:2619
272. Yao X, Tan S, Huang Z, Dong S, Jiang D (2007) Ceram Int 33:901
273. Yoon B-H, Park C-S, Kim H-E, Koh Y-H (2007) J Am Ceram Soc 90:3759
274. Vakifahmetoglu C, Colombo P (2010) In: Colombo P, Raj R (eds) Proceedings of Pac-Rim 8, Advances in polymer derived ceramics and composites: ceramic transactions, vol 213. John Wiley & Sons, pp 95–103
275. Moawad H, Jain H (2007) J Am Ceram Soc 90:1934
276. Moawad H, Jain H (2009) J Mater Sci Mater Med 20:1409
277. Kleebe HJ, Turquat C, Soraru GD (2001) J Am Ceram Soc 84:1073
278. Wilson AM, Zank G, Eguchi K, Xing W, Yates B, Dahn JR (1997) Chem Mater 9:2139
279. Pena-Alonso R, Soraru GD, Raj R (2006) J Am Ceram Soc 89:2473
280. Dibandjo P, Dir Sandra, Babonneau F, Soraru GD (2008) Glass Technol Eur J Glass Sci Technol A 49:175
281. Pena-Alonso R, Mariotto G, Gervais C, Babonneau F, Soraru GD (2007) Chem Mater 19:5694
282. Biasetto L, Peña-Alonso R, Soraru GD, Colombo P (2008) Adv Appl Ceram 107:106
283. Thomas HE (1986) in William S (ed) Applications of refractories: ceramic engineering and science proceedings, applications of refractories: ceramic engineering and science proceedings, vol 7, pp 40-51
284. Shigapov AN, Graham GW, McCabe RW, Paputa Peck M, Kiel Plummer H (1999) Appl Catal B 182:137
285. Gogotsi Y, Nikitin A, Ye H et al (2003) Nat Mater 2:591
286. Yeon S-H, Reddington P, Gogotsi Y, Fischer JE, Vakifahmetoglu C, Colombo P (2010) Carbon 48:201
287. Krawiec P, Schrage C, Kockrick E, Kaskel S (2008) Chem Mater 20:5421
288. Krawiec P, Kockrick E, Borchardt L, Geiger D, Corma A, Kaskel S (2009) J Phys Chem C 113:7755
289. Shi Z-G, Feng Y-Q, Xu L, Da S-L, Zhang M (2003) Carbon 41:2677
290. Xu L-Y, Shi Z-G, Feng Y-Q (2008) Microporous Mesoporous Mater 115:618
291. Kroke E, Li Y-L, Konetschny C, Lecomte E, Fasel C, Riedel R (2000) Mater Sci Eng R 26:97
292. Wan J, Gasch MJ, Mukherjee AK (2001) J Am Ceram Soc 84:2165
293. Belyakov AV, Fomin NN, Koch D (2002) Glass Ceram 59:54
294. Belyakov AV, Fomin NN, Kokh D (2002) Glass Ceram 59: 171
295. Belyakov AV, Fomin NN, Koch D (2003) Glass Ceram 60:14
296. Wilhelm M, Soltmann C, Koch D, Grathwohl G (2005) J Eur Ceram Soc 25:271
297. Wilhelm M, Adam M, Baumer M, Grathwohl G (2008) Adv Eng Mater 10:241
298. Schmidt H, Koch D, Grathwohl G, Colombo P (2001) J Am Ceram Soc 84:2252
299. Heck RM, Gulati S, Farrauto RJ (2001) Chem Eng J 82:149
300. Cybulski A, Moulijn JA (1994) Catal Rev Sci Eng 36:179
301. Giani L, Groppi G, Tronconi E (2005) Ind Eng Chem Res 44:4993
302. Buciuman FC, Kraushaar-Czarnetzki B (2003) Ind Eng Chem Re 42:1863
303. Salvini VR, Innocentini MDM, Pandolfelli VC (2000) Am Ceram Soc Bull 79:49
304. Hartmann M, Vinu A (2002) Langmuir 18:8010
305. Incera Garrido G, Patcas FC, Lang S, Kraushaar-Czarnetzki B (2008) Chem Engin Sci 63:5202
306. Peng Y, Richardson JT (2004) Appl Cat A 266:235
307. Grosse J, Dietrich B, Incera Garrido G, Habisreuther P, Zarzalis N, Martin H, Kind M, Kraushaar-Czarnetzki B (2009) Ind Eng Chem Res 48:10395